A simple a posteriori estimate on general polytopal meshes with applications to complex porous media flows

Martin Vohralík, Soleiman Yousef

A simple a posteriori estimate on general polytopal meshes with applications to complex porous media flows*

Martin Vohralík† Soleiman Yousef‡

June 2, 2017

Abstract

This paper develops an posteriori error estimate for lowest-order locally conservative methods on meshes consisting of very general polytopal elements. We focus on the ease of implementation of the methodology based on H^1-conforming potential reconstruction and $\mathbf{H}(\mathrm{div},\Omega)$-conforming flux reconstruction. In particular, the evaluation of our estimates merely consists in some local matrix-vector multiplications, where, on each mesh element, the matrices are either directly inherited from the given numerical method, or trivially constructed from the element geometry, while the vectors are the degrees of freedom on the given element. We then apply this methodology to unsteady nonlinear coupled degenerate problems describing complex multiphase flows in porous media. Here, on each step of the time-marching scheme, linearization procedure, and linear algebraic solver, we distinguish the corresponding error components. This leads to an easy-to-implement and fast-to-run adaptive algorithm with simultaneously guaranteed overall precision and optimal efficiency ensured through the use of adaptive stopping criteria together with adaptive space and time mesh refinements. Numerous numerical experiments on practical problems in two and three space dimensions illustrate the performance of our methodology.

Key words: A posteriori error estimate, polytopal meshes, stopping criteria, adaptivity, porous media flow

1 Introduction

The use of general polygonal/polyhedral meshes (we henceforth use the term polytopal for any space dimension) is very appealing in various domains in computational practice. In these last years, there has been a growing mathematical background for a priori analysis (existence, uniqueness, convergence, a priori error estimates), see, e.g., Brezzi *et al.* [12], Bazilevs *et al.* [5], Droniou *et al.* [23], Wheeler *et al.* [47], Beirão da Veiga *et al.* [7], Vohralík and Wohlmuth [46], Bonelle and Ern [10], Cangiani *et al.* [16], Cockburn *et al.* [19], and the references therein.

Literature on a posteriori analysis on polytopal meshes is much less plentiful. Beirão da Veiga [6] and Beirão da Veiga and Manzini [8] derive a posteriori error estimates for low-order mimetic finite difference methods; extension to higher-order is presented in Antonietti *et al.* [4]. Arbitrary-order discontinuous Galerkin methods are analysed in Ern and Vohralík [25], relying on the concept of a simplicial submesh. Similarly, Vohralík and Wohlmuth [46] cover at once all the mimetic finite difference, mixed finite volume, hybrid finite volume, and mixed finite element methods on general polytopal meshes. Beirão da Veiga and Manzini [9] then derive a posteriori error estimates for the virtual element method, and Buffa and Giannelli [13] study the isogeometric methods.

The purpose of the present contribution is to derive simple *a posteriori error estimates* applicable on general *polytopal meshes*. Developing the ideas from [25, 46], we do so in a framework including *any*

*This project has partially received funding from the European Research Council (ERC) under the European Union's Horizon 2020 research and innovation program (grant agreement No 647134 GATIPOR).

†Inria Paris, 2 rue Simone Iff, 75589 Paris, France & Université Paris-Est, CERMICS (ENPC), 77455 Marne-la-Vallée, France (martin.vohralik@inria.fr).

‡IFP Energies nouvelles, 1 & 4 av. Bois Préau, 92852 Rueil-Malmaison, France (soleiman.yousef@ifpen.fr).

lowest-order locally conservative method like the mimetic finite difference, mixed finite volume, hybrid finite volume, multi-point finite volume, or mixed finite element ones. Higher-order methods could be treated similarly. Our focus is to derive estimates that can be *easily coded*, *cheaply evaluated*, and *efficiently used* in *practical simulations*. In particular, we want to avoid the physical construction and coding of any simplicial submesh and solution of any local problems. The evaluation of our estimates is fully explicit and merely consists in some small-size matrix-vector multiplications on each mesh element. We either directly use the "element matrices" from the given numerical method, or prescribe them in a simple and explicit way from the geometry of the given element solely. The vectors are then the flux and potential degrees of freedom on the given element. This probably gives the easiest and most practically accessible application to polytopal meshes of the general methodology of H^1-conforming potential reconstruction and $\mathbf{H}(\mathrm{div},\Omega)$-conforming flux reconstruction, see Ern and Vohralík [27] and the references therein.

In the second part of our paper, we apply this methodology to the context of numerical approximation of unsteady nonlinear (systems of) partial differential equations. The derived estimates are still fully computable, featuring no unknown generic constant. They are crucially valid at each stage of the overall solution algorithm: on *each time* step n, each *linearization* step k, and each *linear solver step* i. They also allow to distinguish different *error components* and design *adaptive stopping criteria* for the involved iterative solvers, as well as *adaptive choice* of *space* and *time meshes*. We focus on complex porous media problems, in extension of the results of Ern and Vohralík [26], Vohralík and Wheeler [45], Cancès *et al.* [15], and Di Pietro *et al.* [20, 21].

This contribution is organized as follows. Section 2 sets the context and notation. In Section 3, we develop our main ideas of simple treatment of polytopal meshes on the example of a model steady linear diffusion problem: the single-phase Darcy porous media flow. Numerical illustrations for this case are presented in Section 4. In Section 5, a complex unsteady nonlinear advection-diffusion degenerate system describing a multiphase Darcy flow is treated. A detailed numerical study in this case forms the content of Section 6. Finally, conclusions are drawn in Section 7.

2 Setting

Let $\Omega \subset \mathbb{R}^d$, $d \geq 1$, be an open interval/polygon/polyhedron for respectively $d = 1, 2, 3$, or a polytope in general, with a Lipschitz-continuous boundary $\partial\Omega$. We are interested in partitions $\mathcal{T}_H$ of the domain Ω into polytopes K such that $\cup_{K\in\mathcal{T}_H} K = \overline{\Omega}$. The elements K can in particular be nonconvex, the mesh $\mathcal{T}_H$ can be nonmatching in the sense that intersection of two neighboring polytopal elements is not necessarily their entire face, the maximal number of faces of $K \in \mathcal{T}_H$ is not limited, and there is no condition on $\mathcal{T}_H$ to be shape-regular; we could also easily allow for non star-shaped elements. The only assumption we impose is that there exists a (virtual, not to be constructed in practice) simplicial submesh $\mathcal{T}_h$ of $\mathcal{T}_H$ which is matching, shape-regular, and such that any polytopal element $K \in \mathcal{T}_H$ is covered by a patch of simplices $\mathcal{T}_K$ sharing one vertex of the mesh $\mathcal{T}_h$, which lies in the interior of K. Rephrasing, each element $\kappa \in \mathcal{T}_h$ is a simplex, $\cup_{\kappa\in\mathcal{T}_h} \kappa = \overline{\Omega}$, $\cup_{\kappa\in\mathcal{T}_K} \kappa = K$, $\cup_{K\in\mathcal{T}_H} \mathcal{T}_K = \mathcal{T}_h$, the intersection of two elements in $\mathcal{T}_h$ is either empty or their d'-dimensional common face, $0 \leq d' \leq d-1$, and the ratios of the diameter of each $\kappa \in \mathcal{T}_h$ to the diameter of its largest inscribed ball are uniformly bounded by a constant $\theta_{\mathcal{T}} > 0$ for all considered meshes $\{\mathcal{T}_H\}_H$. An illustration in two dimensions is provided in Figure 1.

Let $\mathcal{E}_H$ be the set of the $(d-1)$-dimensional faces of $\mathcal{T}_H$, divided into interior faces $\mathcal{E}_H^{\mathrm{int}}$ and boundary faces $\mathcal{E}_H^{\mathrm{ext}}$: $\sigma \in \mathcal{E}_H^{\mathrm{int}}$ if there exist $K, K' \in \mathcal{T}_H$, $K \neq K'$, such that $\sigma = K \cap K'$, and $\sigma \in \mathcal{E}_H^{\mathrm{ext}}$ if there exist $K \in \mathcal{T}_H$ such that $\sigma = K \cap \partial\Omega$. Similarly, let $\mathcal{E}_h$ be the set of the $(d-1)$-dimensional faces of the simplicial mesh $\mathcal{T}_h$. We denote by $\mathcal{E}_{H,h}$ the set of such faces from $\mathcal{E}_h$ that lie in some polytopal face of $\mathcal{E}_H$. If the faces of $\mathcal{T}_h$ do not subdivide the faces of $\mathcal{T}_H$, then $\mathcal{E}_{H,h} = \mathcal{E}_H$. Let $\mathcal{E}_K \subset \mathcal{E}_H$ be the set of the $(d-1)$-dimensional faces of the polytope $K \in \mathcal{T}_H$. Then, we let $\mathcal{E}_{K,h}^{\mathrm{ext}}$ collect those faces of $\mathcal{E}_{H,h}$ that lie on the boundary of the element $K \in \mathcal{T}_H$, whereas $\mathcal{E}_{K,h}^{\mathrm{int}}$ those faces of $\mathcal{E}_{H,h}$ that lie inside the element $K \in \mathcal{T}_H$, see Figure 1. To complete the notation, we also let $\mathcal{V}_h$ be the set of the vertices of the mesh $\mathcal{T}_h$, $\mathcal{V}_\sigma$ vertices of the face $\sigma \in \mathcal{E}_h$, $\mathcal{V}_K$ vertices of the element $K \in \mathcal{T}_H$, and $\mathcal{V}_{K,h}$ the vertices of the elements $\kappa \in \mathcal{T}_K$.

For a set $\mathcal{S}$, $|\mathcal{S}|$ henceforth stands for its cardinality. We also use the notation $|K|$ for the Lebesgue measure of an element K and $|\sigma|$ for the $(d-1)$-dimensional Lebesgue measure of a face σ. For an interior face $\sigma \in \mathcal{E}_H^{\mathrm{int}}$, we fix an arbitrary orientation and denote the corresponding unit normal vector by $\mathbf{n}_\sigma$. For a boundary face $\sigma \in \mathcal{E}_H^{\mathrm{ext}}$, $\mathbf{n}_\sigma$ coincides with the exterior unit normal $\mathbf{n}_\Omega$ of Ω. Finally, for all $K \in \mathcal{T}_H$ and all

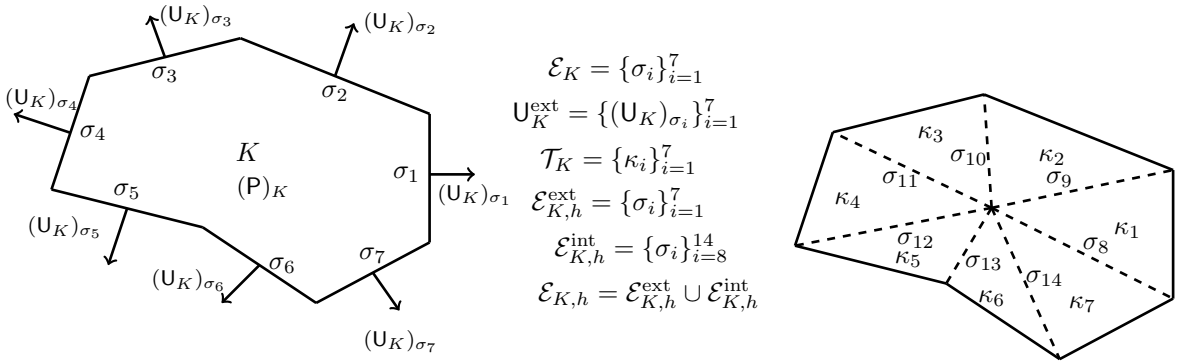

Figure 1: Example of a general polygonal element K with its faces $\mathcal{E}_K$, corresponding face fluxes $\mathsf{U}_K^{\rm ext}$, and pressure head $(\mathsf{P})_K$ (left); virtual simplicial submesh $\mathcal{T}_K$ of K (right)

$\sigma \in \mathcal{E}_K$, we denote by $\mathbf{n}_{K,\sigma}$ the unit normal vector to σ pointing out of K. In what follows, we will often use the local weighted norm on $K \in \mathcal{T}_H$, for $\mathbf{v} \in \left[L^2(K)\right]^d$:

$$\|\mathbf{v}\|_{\underline{\mathbf{K}}^{-\frac{1}{2}};L^2(K)} := \left\|\underline{\mathbf{K}}^{-\frac{1}{2}}\mathbf{v}\right\|_{L^2(K)} = \left\{\int_K |(\underline{\mathbf{K}}^{-\frac{1}{2}}(\mathbf{x})\mathbf{v}(\mathbf{x}))|^2 \,\mathrm{d}\mathbf{x}\right\}^{\frac{1}{2}}.$$

3 A model steady linear problem

We describe here first a simple model steady linear problem together with its generic locally conservative polytopal discretization. Then our a posteriori estimates, relying on the methodology of flux and potential reconstructions where we avoid their factual construction, are described.

3.1 Steady linear Darcy flow

Consider the problem of finding $p : \Omega \to \mathbb{R}$ such that

$$-\nabla\cdot(\underline{\mathbf{K}}\nabla p) = f \qquad \text{in } \Omega, \tag{3.1a}$$
$$p = 0 \qquad \text{on } \partial\Omega. \tag{3.1b}$$

Here f is the source term and $\underline{\mathbf{K}}$ is a positive definite diffusion-dispersion tensor with values in $\mathbb{R}^{d\times d}$; we suppose for simplicity that they are both piecewise constant with respect to the mesh $\mathcal{T}_H$. In weak form, (3.1) amounts to looking for $p \in H_0^1(\Omega)$ such that

$$(\underline{\mathbf{K}}\nabla p, \nabla v) = (f, v) \qquad \forall v \in H_0^1(\Omega). \tag{3.2}$$

From the pressure head p, we can define the Darcy velocity

$$\mathbf{u} := -\underline{\mathbf{K}}\nabla p, \tag{3.3}$$

and it follows from (3.2) that $\mathbf{u}$ lies in $\mathbf{H}(\mathrm{div}, \Omega)$ and is such that $\nabla\cdot\mathbf{u} = f$.

3.2 A generic discretization on a polytopal mesh

Let $\mathcal{T}_H$ be a polytopal mesh of Ω satisfying the assumptions of Section 2. We consider in this paper any scheme that can be written under the following abstract form:

Assumption 3.1 (Locally conservative discretization on a polytopal mesh)**.** *There holds:*

1. *There is one unknown* $(\mathsf{U})_\sigma \in \mathbb{R}$ *per face* $\sigma \in \mathcal{E}_H$ *and one unknown* $(\mathsf{P})_K \in \mathbb{R}$ *per element* $K \in \mathcal{T}_H$. *They respectively approximate the normal flux* $\langle \mathbf{u}\cdot\mathbf{n}_\sigma, 1\rangle_\sigma$ *and the pressure head* p *in the element* K.

2. *The flux balance*
$$\sum_{\sigma\in\mathcal{E}_K} (\mathsf{U})_\sigma \mathbf{n}_{K,\sigma}\cdot\mathbf{n}_\sigma = (\mathsf{F})_K, \quad \forall K \in \mathcal{T}_H, \tag{3.4}$$
is satisfied, where $(\mathsf{F})_K := (f,1)_K$.

Many lowest-order locally conservative methods take the following specific form contained in Assumption 3.1, see in particular [46, Theorems 7.2 and 7.3] for the relation to mixed finite elements:

Remark 3.2 (Saddle-point discretization on a polytopal mesh)**.** *Find* $\mathsf{U} := \{(\mathsf{U})_\sigma\}_{\sigma\in\mathcal{E}_H} \in \mathbb{R}^{|\mathcal{E}_H|}$ *and* $\mathsf{P} := \{(\mathsf{P})_K\}_{K\in\mathcal{T}_H} \in \mathbb{R}^{|\mathcal{T}_H|}$ *such that*
$$\begin{pmatrix} \mathbb{A} & \mathbb{B}^{\mathrm{t}} \\ \mathbb{B} & 0 \end{pmatrix} \begin{pmatrix} \mathsf{U} \\ \mathsf{P} \end{pmatrix} = \begin{pmatrix} 0 \\ \mathsf{F} \end{pmatrix}, \tag{3.5}$$
where 1) $\mathbb{B}$ *has a full rank; 2) for* $K \in \mathcal{T}_H$ *and* $\sigma \in \mathcal{E}_H$, $\mathbb{B}_{K,\sigma} = -\mathbf{n}_{K,\sigma}\cdot\mathbf{n}_\sigma$ *if* $\sigma \in \mathcal{E}_K$ *and* $\mathbb{B}_{K,\sigma} = 0$ *otherwise; 2)* $\mathbb{A}$ *is square and invertible; 3)* $\widehat{\mathbb{A}}_K \in \mathbb{R}^{|\mathcal{E}_K|\times|\mathcal{E}_K|}$ *are the "element matrices" of the given method; 4) for* $\sigma,\sigma' \in \mathcal{E}_H$, $\mathbb{A}_{\sigma,\sigma'} = 0$ *if* σ *and* σ' *are not faces of the same element* $K \in \mathcal{T}_H$ *and* $\mathbb{A}_{\sigma,\sigma'} = \sum_{K\in\mathcal{T}_H,\{\sigma,\sigma'\}\in\mathcal{E}_K} \mathbf{n}_{K,\sigma}\cdot\mathbf{n}_\sigma \mathbf{n}_{K,\sigma'}\cdot\mathbf{n}_{\sigma'} (\widehat{\mathbb{A}}_K)_{\sigma,\sigma'}$ *otherwise; 5)* $\mathsf{F} := \{(\mathsf{F})_K\}_{K\in\mathcal{T}_H} \in \mathbb{R}^{|\mathcal{T}_H|}$.

3.3 A fictitious flux reconstruction

Following the general concept of the lifting operator in mimetic finite differences, see, e.g., [12, Theorem 5.1], [6, Section 2.1], or [8, Section 2.4], see also Eymard *et al.* [28, Section 1.2], Kuznetsov and Repin [32], Kuznetsov [33], Vohralík [43, Section 3.2], or Sboui *et al.* [40], we will now extend the fluxes $(\mathsf{U})_\sigma$, $\sigma \in \mathcal{E}_K$, to the interior of each polytopal element $K \in \mathcal{T}_H$. The obtained flux $\mathbf{u}_h|_K$ will be used for the purpose of our a posteriori analysis, but is crucially not to be constructed in practice. We will more precisely proceed following [46, Theorems 7.2 and 7.3], where we approximate by the mixed finite element method on the simplicial mesh $\mathcal{T}_K$ of each element $K \in \mathcal{T}_H$ the problem
$$-\nabla\cdot(\underline{\mathbf{K}}\nabla p_K) = f|_K, \tag{3.6a}$$
$$\frac{(p_K,1)_K}{|K|} = (\mathsf{P})_K, \tag{3.6b}$$
$$-\underline{\mathbf{K}}\nabla p_K\cdot\mathbf{n}_{\sigma'} = \frac{(\mathsf{U})_\sigma}{|\sigma|} \quad \forall \sigma' \in \mathcal{E}_{K,h}^{\mathrm{ext}},\ \sigma' \subset \sigma,\ \sigma \in \mathcal{E}_K. \tag{3.6c}$$
Note that if the faces of the simplicial mesh $\mathcal{T}_h$ do not subdivide the faces of the polytopal mesh $\mathcal{T}_H$, then $\mathcal{E}_{K,h}^{\mathrm{ext}} = \mathcal{E}_K$, so that it is enough to consider directly all faces $\sigma' \in \mathcal{E}_K$ in (3.6c). Henceforth, we will also use the notation
$$(\mathsf{U})_{\sigma'} := \frac{(\mathsf{U})_\sigma}{|\sigma|}|\sigma'| \quad \forall \sigma' \in \mathcal{E}_{K,h}^{\mathrm{ext}},\ \sigma' \subset \sigma,\ \sigma \in \mathcal{E}_K \tag{3.7}$$
for the normal flux over the given simplicial subface σ' of each original polytopal face σ.

For each polytope $K \in \mathcal{T}_H$, define the lowest-order Raviart–Thomas–Nédélec space $\mathbf{RTN}_0(K) := \{\mathbf{v}_h \in \mathbf{H}(\mathrm{div},K);\ \mathbf{v}_h|_\kappa \in [\mathbb{P}_0(\kappa)]^d + \mathbf{x}\mathbb{P}_0(\kappa)\ \forall \kappa \in \mathcal{T}_K\}$ over the simplicial submesh $\mathcal{T}_K$ of K. Here $\mathbb{P}_0(\kappa)$ stands for constants on the simplex κ, and we will also denote by $\mathbb{P}_0(\mathcal{T}_K)$ the space of piecewise constants on the polytope K with respect to its mesh $\mathcal{T}_K$. We then set
$$\begin{aligned}
&\mathbf{V}_{h,\mathrm{N}}^K := \{\mathbf{v}_h \in \mathbf{RTN}_0(K),\ \langle \mathbf{v}_h\cdot\mathbf{n}_\sigma, 1\rangle_\sigma = (\mathsf{U})_\sigma\ \forall \sigma \in \mathcal{E}_{K,h}^{\mathrm{ext}}\},\\
&\mathbf{V}_{h,0}^K := \{\mathbf{v}_h \in \mathbf{RTN}_0(K),\ \langle \mathbf{v}_h\cdot\mathbf{n}_\sigma, 1\rangle_\sigma = 0\ \forall \sigma \in \mathcal{E}_{K,h}^{\mathrm{ext}}\},\\
&Q_{h,\mathrm{N}}^K := \{q_h \in \mathbb{P}_0(\mathcal{T}_K);\ \tfrac{(q_h,1)_K}{|K|} = (\mathsf{P})_K\},\\
&Q_{h,0}^K := \{q_h \in \mathbb{P}_0(\mathcal{T}_K);\ (q_h,1)_K = 0\}.
\end{aligned}$$

Definition 3.3 (Element fictitious flux reconstruction)**.** *For $K \in \mathcal{T}_H$, define $\mathbf{u}_h|_K \in \mathbf{V}_{h,\mathrm{N}}^K$ and $p_h|_K \in Q_{h,\mathrm{N}}^K$ by*

$$(\underline{\mathbf{K}}^{-1}\mathbf{u}_h, \mathbf{v}_h)_K - (p_h, \nabla\cdot\mathbf{v}_h)_K = 0 \qquad \forall \mathbf{v}_h \in \mathbf{V}_{h,0}^K, \tag{3.8a}$$

$$-(\nabla\cdot\mathbf{u}_h, q_h)_K = 0 \qquad \forall q_h \in Q_{h,0}^K. \tag{3.8b}$$

It is worth noting that $(f, q_h)_K = 0$ for all $q_h \in Q_{h,0}^K$, so that the right-hand side in (3.8b) is indeed zero; this follows from the zero mean value constraint on the test function q_h together with the assumption that the source term f is constant on each K. Note also that since the normal fluxes $(\mathsf{U})_\sigma$ are univalued on the faces from $\mathcal{E}_{H,h}$, the resulting flux reconstruction $\mathbf{u}_h$ has the normal trace continuous and thus belongs to the Raviart–Thomas–Nédélec space $\mathbf{RTN}_0(\Omega)$ associated with the simplicial mesh $\mathcal{T}_h$ of the entire domain Ω. In matrix form, Definition 3.3 takes the following form:

Remark 3.4 (Matrix form of (3.8))**.** *Let $\mathbf{v}_\sigma$, $\sigma \in \mathcal{E}_{K,h}^{\mathrm{int}}$, be the basis functions of the space $\mathbf{V}_{h,0}^K$, and $\mathbf{v}_\sigma$, $\sigma \in \mathcal{E}_{K,h}^{\mathrm{ext}}$, be the remaining basis functions of the space $\mathbf{RTN}_0(K)$. Similarly, let q_i, $1 \le i \le |Q_{h,0}^K|$, be the basis functions of the space $Q_{h,0}^K$. Consider these basis functions of $\mathbf{V}_{h,0}^K$ and $Q_{h,0}^K$ as test functions in (3.8) and develop $\mathbf{u}_h|_K = \sum_{\sigma\in\mathcal{E}_{K,h}^{\mathrm{ext}}} (\mathsf{U}_K^{\mathrm{ext}})_\sigma \mathbf{v}_\sigma + \sum_{\sigma\in\mathcal{E}_{K,h}^{\mathrm{int}}} (\mathsf{U}_K^{\mathrm{int}})_\sigma \mathbf{v}_\sigma$ and $p_h|_K = (\mathsf{P})_K + \sum_{i=1}^{|Q_{h,0}^K|} (\mathsf{P}_K^0)_i q_i$, where $\mathsf{U}_K^{\mathrm{ext}} := \{(\mathsf{U})_\sigma\}_{\sigma\in\mathcal{E}_{K,h}^{\mathrm{ext}}}$ and $(\mathsf{P})_K$ are the given data of the problem (3.6). Then (3.8) in matrix form corresponds to: find $\mathsf{U}_K^{\mathrm{int}} \in \mathbb{R}^{|\mathbf{V}_{h,0}^K|}$ and $\mathsf{P}_K^0 \in \mathbb{R}^{|Q_{h,0}^K|}$ such that*

$$\begin{pmatrix} \mathbb{A}_K^{\mathrm{int,int}} & (\mathbb{B}_K^{0,\mathrm{int}})^{\mathrm{t}} \\ \mathbb{B}_K^{0,\mathrm{int}} & 0 \end{pmatrix} \begin{pmatrix} \mathsf{U}_K^{\mathrm{int}} \\ \mathsf{P}_K^0 \end{pmatrix} = \begin{pmatrix} -\mathbb{A}_K^{\mathrm{int,ext}}\mathsf{U}_K^{\mathrm{ext}} \\ -\mathbb{B}_K^{0,\mathrm{ext}}\mathsf{U}_K^{\mathrm{ext}} \end{pmatrix}, \tag{3.9}$$

where

$$\begin{aligned} (\mathbb{A}_K^{\mathrm{int,int}})_{\sigma,\sigma'} &:= (\underline{\mathbf{K}}^{-1}\mathbf{v}_{\sigma'}, \mathbf{v}_\sigma)_K \qquad \sigma,\sigma' \in \mathcal{E}_{K,h}^{\mathrm{int}}, \\ (\mathbb{A}_K^{\mathrm{int,ext}})_{\sigma,\sigma'} &:= (\underline{\mathbf{K}}^{-1}\mathbf{v}_{\sigma'}, \mathbf{v}_\sigma)_K \qquad \sigma \in \mathcal{E}_{K,h}^{\mathrm{int}}, \sigma' \in \mathcal{E}_{K,h}^{\mathrm{ext}}, \\ (\mathbb{B}_K^{0,\mathrm{int}})_{K,\sigma} &:= -\mathbf{n}_{K,\sigma}\mathbf{n}_\sigma \qquad \sigma \in \mathcal{E}_{K,h}^{\mathrm{int}}, \\ (\mathbb{B}_K^{0,\mathrm{ext}})_{K,\sigma} &:= -\mathbf{n}_{K,\sigma}\mathbf{n}_\sigma \qquad \sigma \in \mathcal{E}_{K,h}^{\mathrm{ext}}. \end{aligned}$$

Definition 3.3 employs the mixed finite element method to lift the information from the boundary of an element $K \in \mathcal{T}_H$ given by the fluxes $\mathsf{U}_K^{\mathrm{ext}}$ to the interior of the element K. It is thus clear that the energy $\|\mathbf{u}_h\|_{\underline{\mathbf{K}}^{-\frac{1}{2}};L^2(K)}$ needs to only depend on $\mathsf{U}_K^{\mathrm{ext}}$. It turns out that link can be expressed by the *element matrix* $\widehat{\mathbb{A}}_{\mathrm{MFE},K}$. Define, in addition to Remark 3.4,

$$(\mathbb{A}_K^{\mathrm{ext,ext}})_{\sigma,\sigma'} := (\underline{\mathbf{K}}^{-1}\mathbf{v}_{\sigma'}, \mathbf{v}_\sigma)_K \qquad \sigma,\sigma' \in \mathcal{E}_{K,h}^{\mathrm{ext}}.$$

As in [46, proof of Theorem 7.3], we indeed have:

Lemma 3.5 (MFE element matrix and energy norm)**.** *For each polytopal element $K \in \mathcal{T}_H$, define the element matrix of the mixed finite element method*

$$\widehat{\mathbb{A}}_{\mathrm{MFE},K} := \mathbb{A}_K^{\mathrm{ext,ext}} - \begin{pmatrix} \mathbb{A}_K^{\mathrm{int,ext}} \\ \mathbb{B}_K^{0,\mathrm{ext}} \end{pmatrix}^{\mathrm{t}} \begin{pmatrix} \mathbb{A}_K^{\mathrm{int,int}} & (\mathbb{B}_K^{0,\mathrm{int}})^{\mathrm{t}} \\ \mathbb{B}_K^{0,\mathrm{int}} & 0 \end{pmatrix}^{-1} \begin{pmatrix} \mathbb{A}_K^{\mathrm{int,ext}} \\ \mathbb{B}_K^{0,\mathrm{ext}} \end{pmatrix}. \tag{3.10}$$

Let $\mathbf{u}_h|_K \in \mathbf{V}_{h,\mathrm{N}}^K$ be given by Definition 3.3. Then

$$\|\mathbf{u}_h\|^2_{\underline{\mathbf{K}}^{-\frac{1}{2}};L^2(K)} = (\mathsf{U}_K^{\mathrm{ext}})^{\mathrm{t}}\widehat{\mathbb{A}}_{\mathrm{MFE},K}\mathsf{U}_K^{\mathrm{ext}}. \tag{3.11}$$

Proof. Let $K \in \mathcal{T}_H$. Following Remark 3.4, decompose $\mathbf{u}_h|_K = \mathbf{u}_{h,K}^{\mathrm{ext}} + \mathbf{u}_{h,K}^{\mathrm{int}}$ and $p_h|_K = (\mathsf{P})_K + p_{h,K}^0$. Note that choosing $\mathbf{u}_{h,K}^{\mathrm{int}} \in \mathbf{V}_{h,0}^K$ as the test function in (3.8a) and $p_{h,K}^0 \in Q_{h,0}^K$ as the test function in (3.8b), one has

$$(\underline{\mathbf{K}}^{-1}\mathbf{u}_h, \mathbf{u}_{h,K}^{\mathrm{int}})_K = (p_{h,K}^0, \nabla\cdot\mathbf{u}_{h,K}^{\mathrm{int}})_K = -(p_{h,K}^0, \nabla\cdot\mathbf{u}_{h,K}^{\mathrm{ext}})_K,$$

where we have used $((\mathsf{P})_K, \nabla\cdot\mathbf{u}_{h,K}^{\mathrm{int}})_K = 0$. Consequently,

$$\begin{aligned}\|\mathbf{u}_h\|^2_{\underline{\mathbf{K}}^{-\frac{1}{2}};L^2(K)} &= (\underline{\mathbf{K}}^{-1}\mathbf{u}_h, \mathbf{u}_h)_K \\ &= (\underline{\mathbf{K}}^{-1}\mathbf{u}_h, \mathbf{u}_h^{\mathrm{int}})_K + (\underline{\mathbf{K}}^{-1}\mathbf{u}_h^{\mathrm{int}}, \mathbf{u}_h^{\mathrm{ext}})_K + (\underline{\mathbf{K}}^{-1}\mathbf{u}_h^{\mathrm{ext}}, \mathbf{u}_h^{\mathrm{ext}})_K \\ &= -(p_{h,K}^0, \nabla\cdot\mathbf{u}_{h,K}^{\mathrm{ext}})_K + (\underline{\mathbf{K}}^{-1}\mathbf{u}_h^{\mathrm{int}}, \mathbf{u}_h^{\mathrm{ext}})_K + (\underline{\mathbf{K}}^{-1}\mathbf{u}_h^{\mathrm{ext}}, \mathbf{u}_h^{\mathrm{ext}})_K \\ &= (\mathsf{U}_K^{\mathrm{ext}})^{\mathrm{t}} \begin{pmatrix} \mathbb{A}_K^{\mathrm{int,ext}} \\ \mathbb{B}_K^{0,\mathrm{ext}} \end{pmatrix}^{\mathrm{t}} \begin{pmatrix} \mathsf{U}_K^{\mathrm{int}} \\ \mathsf{P}_K^0 \end{pmatrix} + (\mathsf{U}_K^{\mathrm{ext}})^{\mathrm{t}} \mathbb{A}_K^{\mathrm{ext,ext}} \mathsf{U}_K^{\mathrm{ext}}.\end{aligned}$$

Combining this with the MFE matrix form (3.9) and the MFE element matrix definition (3.10) finishes the proof. □

Remark 3.6 (Given discretization scheme element matrix and energy norm)**.** *The unified analysis in [46] together with the results of [12, 23] show that the mixed finite element element matrix $\widehat{\mathbb{A}}_{\mathrm{MFE},K}$ defined by (3.10) belongs to the same family as the element matrices $\widehat{\mathbb{A}}_K$ of mimetic finite differences, mixed finite volumes, and hybrid finite volumes. Thus, for any discretization scheme of the form of Remark 3.2, a simple approximate way to evaluate $\|\mathbf{u}_h\|^2_{\underline{\mathbf{K}}^{-\frac{1}{2}};L^2(K)}$ in (3.11) is to replace the element matrix $\widehat{\mathbb{A}}_{\mathrm{MFE},K}$ of the mixed finite element method by the matrix $\widehat{\mathbb{A}}_K$ available from the given discretization scheme. In other words: for the normal face fluxes $\mathsf{U}_K^{\mathrm{ext}} = \{(\mathsf{U})_\sigma\}_{\sigma\in\mathcal{E}_{K,h}^{\mathrm{ext}}}$ given by a scheme of the form (3.5) and for $\mathbf{u}_h|_K \in \mathbf{V}_{h,\mathrm{N}}^K$ prescribed therefrom by Definition 3.3, there holds*

$$\|\mathbf{u}_h\|^2_{\underline{\mathbf{K}}^{-\frac{1}{2}};L^2(K)} \approx (\mathsf{U}_K^{\mathrm{ext}})^{\mathrm{t}} \widehat{\mathbb{A}}_K \mathsf{U}_K^{\mathrm{ext}}, \tag{3.12}$$

where $\widehat{\mathbb{A}}_K$ is the element matrix of the given scheme specified in Remark 3.2. Finally, when replacing the discrete $\mathbf{u}_h \in \mathbf{V}_{h,\mathrm{N}}^K$ of Definition 3.3 by the continuous $\tilde{\mathbf{u}}_h \in \mathbf{H}(\mathrm{div}, K)$ of the lifting operator according to [12, Theorem 5.1]

$$\|\tilde{\mathbf{u}}_h\|^2_{\underline{\mathbf{K}}^{-\frac{1}{2}};L^2(K)} = (\mathsf{U}_K^{\mathrm{ext}})^{\mathrm{t}} \widehat{\mathbb{A}}_K \mathsf{U}_K^{\mathrm{ext}}, \tag{3.13}$$

where now $\tilde{\mathbf{u}}_h$ is typically not accessible in practice, similarly to [6, 8].

3.4 A fictitious potential reconstruction

As a second ingredient of our a posteriori analysis, we will now define a simple potential reconstruction $s_h \in \mathbb{P}_1(\mathcal{T}_h) \cap H_0^1(\Omega)$, piecewise affine with respect to the simplicial submesh $\mathcal{T}_h$ and $H_0^1(\Omega)$-conforming. Crucially, it also fictitious in the sense that it does not need to be constructed in practice in order to evaluate the resulting a posteriori error estimate.

In the spirit of usual averaging operators [24, 2, 31, 3, 14], the easiest way is to set the nodal values $s_h(\mathbf{a})$ in the vector $\{(\mathsf{S})_\mathbf{a}\}_{\mathbf{a}\in\mathcal{V}_h}$ by average values of $(\mathsf{P})_K$ in the neighboring elements:

Definition 3.7 (Element potential reconstruction)**.** *For each polytopal element $K \in \mathcal{T}_H$ and each vertex $\mathbf{a}$ of the simplicial mesh $\mathcal{T}_h$ lying on ∂K but not on $\partial\Omega$, let $\mathcal{T}_\mathbf{a}$ denote the set of polytopal elements $K \in \mathcal{T}_H$ sharing $\mathbf{a}$. We set*

$$(\mathsf{S})_\mathbf{a} := (\mathsf{S}_K)_\mathbf{a} := \frac{1}{|\mathcal{T}_\mathbf{a}|} \sum_{K\in\mathcal{T}_\mathbf{a}} (\mathsf{P})_K. \tag{3.14}$$

We also set $(\mathsf{S})_\mathbf{a} := (\mathsf{S}_K)_\mathbf{a} := (\mathsf{P})_K$ for the vertex $\mathbf{a}$ of $\mathcal{T}_h$ lying inside $K \in \mathcal{T}_H$ and $(\mathsf{S})_\mathbf{a} := (\mathsf{S}_K)_\mathbf{a} := 0$ for any vertex $\mathbf{a}$ lying simultaneously on ∂K and the domain boundary $\partial\Omega$.

For each $K \in \mathcal{T}_H$, let $\mathsf{S}_K \in \mathbb{R}^{|\mathcal{V}_{K,h}|}$ collect the values $(\mathsf{S}_K)_\mathbf{a}$ for the vertices $\mathbf{a}$ of the simplicial mesh $\mathcal{T}_K$ lying on the boundary ∂K and the value inside K. We will also need the vector $\mathsf{S}_K^{\mathrm{ext}} \in \mathbb{R}^{|\mathcal{E}_{K,h}^{\mathrm{ext}}|}$ collecting the values associated with faces $\sigma \in \mathcal{E}_{K,h}^{\mathrm{ext}}$ that we prescribe by

$$(\mathsf{S}_K^{\mathrm{ext}})_\sigma := \frac{1}{d} \sum_{\mathbf{a}\in\mathcal{V}_\sigma} (\mathsf{S})_\mathbf{a}, \tag{3.15}$$

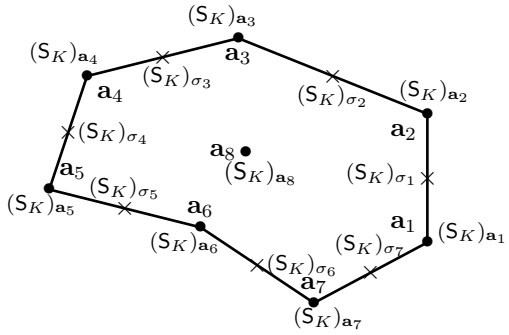

Figure 2: Example of nodal and facial potential reconstruction values S_K and $\mathsf{S}_K^{\rm ext}$

where, recall, $\mathcal{V}_\sigma$ collects the vertices of the given face $\sigma \in \mathcal{E}_{K,h}^{\rm ext}$. Note that $(\mathsf{S}_K^{\rm ext})_\sigma = s_h(\mathbf{x}_\sigma)$, i.e., it is the punctual value of the reconstruction s_h in the face barycenter $\mathbf{x}_\sigma$, $\sigma \in \mathcal{E}_{K,h}^{\rm ext}$. Figure 2 gives an illustration of the vectors S_K and $\mathsf{S}_K^{\rm ext}$ in two space dimensions.

Consider the usual hat basis functions $\psi_{\mathbf{a}}$ on the simplicial mesh $\mathcal{T}_h$. Here $\psi_{\mathbf{a}}$ is piecewise affine on $\mathcal{T}_h$ and $H_0^1(\Omega)$-conforming, $\psi_{\mathbf{a}}(\mathbf{a}') = 1$ if $\mathbf{a} = \mathbf{a}'$ and 0 otherwise, where $\mathbf{a}, \mathbf{a}' \in \mathcal{V}_h$ are the vertices of $\mathcal{T}_h$. We will need below the *stiffness matrix* $\widehat{\mathbb{S}}_{{\rm FE},K} \in \mathbb{R}^{|\mathcal{V}_{K,h}|\times|\mathcal{V}_{K,h}|}$ of a polytopal element $K \in \mathcal{T}_H$ by

$$(\widehat{\mathbb{S}}_{{\rm FE},K})_{\mathbf{a},\mathbf{a}'} := (\underline{\mathbf{K}}\nabla\psi_{\mathbf{a}'}, \nabla\psi_{\mathbf{a}})_K \qquad \mathbf{a}, \mathbf{a}' \in \mathcal{V}_{K,h}. \tag{3.16}$$

An immediate consequence is that

$$\|\underline{\mathbf{K}}\nabla s_h\|_{\underline{\mathbf{K}}^{-\frac12};L^2(K)}^2 = \mathsf{S}_K{}^{\rm t}\widehat{\mathbb{S}}_{{\rm FE},K}\mathsf{S}_K. \tag{3.17}$$

Similarly, we let the element *mass matrix* $\widehat{\mathbb{M}}_{{\rm FE},K} \in \mathbb{R}^{|\mathcal{V}_{K,h}|\times|\mathcal{V}_{K,h}|}$ be given by

$$(\widehat{\mathbb{M}}_{{\rm FE},K})_{\mathbf{a},\mathbf{a}'} := (\psi_{\mathbf{a}'}, \psi_{\mathbf{a}})_K \qquad \mathbf{a}, \mathbf{a}' \in \mathcal{V}_{K,h}. \tag{3.18}$$

Then

$$(1, s_h)_K = 1^{\rm t}\widehat{\mathbb{M}}_{{\rm FE},K}\mathsf{S}_K. \tag{3.19}$$

Remark 3.8 (Element matrices $\widehat{\mathbb{S}}_{{\rm FE},K}$ and $\widehat{\mathbb{M}}_{{\rm FE},K}$)**.** *The stiffness and mass finite element matrices $\widehat{\mathbb{S}}_{{\rm FE},K}$ of (3.16) and $\widehat{\mathbb{M}}_{{\rm FE},K}$ of (3.18) are available via simple analytical formulas that merely necessitate the position of the vertices in the simplicial mesh $\mathcal{T}_K = \mathcal{T}_h|_K$ of each element $K \in \mathcal{T}_H$. Thus neither $\mathcal{T}_h$ nor $\mathcal{T}_K$ need not be constructed in practice in order to obtain them.*

We finish this section by several remarks concerning saddle-point discretizations of the form (3.5) of Remark 3.2.

Remark 3.9 (Lagrange multipliers in saddle-point discretizations)**.** *As usual for locally conservative methods, cf. Roberts and Thomas [39], Brezzi and Fortin [11], or Droniou* et al. *[23], the formulation (3.5) can be hybridized, giving rise to one Lagrange multiplier Λ_σ per face $\sigma \in \mathcal{E}_H$. Consider the line associated with a given $\sigma \in \mathcal{E}_H$ in the first block equation of (3.5). For an interior face σ, let it be shared by two polytopes $K, K' \in \mathcal{T}_H$ such that $\mathbf{n}_\sigma$ points from K to K'. From the structure of the matrices $\mathbb{A}$ and $\mathbb{B}$ supposed in Remark 3.2, it follows that*

$$\sum_{\sigma'\in\mathcal{E}_K} \mathbf{n}_{K,\sigma'}\cdot\mathbf{n}_{\sigma'}(\widehat{\mathbb{A}}_K)_{\sigma,\sigma'}(\mathsf{U})_{\sigma'} - (\mathsf{P})_K = \sum_{\sigma'\in\mathcal{E}_{K'}} \mathbf{n}_{K',\sigma'}\cdot\mathbf{n}_{\sigma'}(\widehat{\mathbb{A}}_K)_{\sigma,\sigma'}(\mathsf{U})_{\sigma'} - (\mathsf{P})_{K'},$$

so that these expressions are univalued from both elements K and K'. As such an expression is also clearly univalued on boundary faces, we can define the Lagrange multipliers

$$\Lambda_\sigma := (\mathsf{P})_K - \sum_{\sigma'\in\mathcal{E}_K} \mathbf{n}_{K,\sigma'}\cdot\mathbf{n}_{\sigma'}(\widehat{\mathbb{A}}_K)_{\sigma,\sigma'}(\mathsf{U})_{\sigma'} \tag{3.20}$$

for each element $K \in \mathcal{T}_H$ and each face $\sigma \in \mathcal{E}_K$.

For saddle-point discretizations of Remark 3.2, we can thus use the Lagrange multipliers Λ_σ given by (3.20) to define a more accurate fictitious potential reconstruction s_h, still piecewise affine with respect to the simplicial submesh $\mathcal{T}_h$ and $H^1_0(\Omega)$-conforming. We impose the nodal values $s_h(\mathbf{a})$ in the vector $\{(\mathsf{S})_\mathbf{a}\}_{\mathbf{a}\in\mathcal{V}_h}$ by averaging the values Λ_σ:

Definition 3.10 (Element potential reconstruction based on Lagrange multipliers)**.** *For each polytopal element $K \in \mathcal{T}_H$ and each vertex $\mathbf{a}$ of the simplicial mesh $\mathcal{T}_K$ lying on ∂K but not on the boundary $\partial\Omega$ and shared by faces from $\mathcal{E}_K$ collected in the set $\mathcal{E}_{K,\mathbf{a}}$, define first $(\bar{\mathsf{S}})_\mathbf{a} := (\bar{\mathsf{S}}_K)_\mathbf{a} := \frac{1}{|\mathcal{E}_{K,\mathbf{a}}|}\sum_{\sigma\in\mathcal{E}_{K,\mathbf{a}}}\Lambda_\sigma$. On the boundary $\partial\Omega$, define $(\bar{\mathsf{S}})_\mathbf{a} := (\bar{\mathsf{S}}_K)_\mathbf{a} := 0$. Let now a vertex $\mathbf{a}$ of the simplicial mesh $\mathcal{T}_h$ lie on ∂K for some $K \in \mathcal{T}_H$ and let $\mathcal{T}_\mathbf{a}$ denote the elements $K \in \mathcal{T}_H$ sharing $\mathbf{a}$. We then set*

$$(\mathsf{S})_\mathbf{a} := (\mathsf{S}_K)_\mathbf{a} := \frac{1}{|\mathcal{T}_\mathbf{a}|}\sum_{K\in\mathcal{T}_\mathbf{a}}(\bar{\mathsf{S}}_K)_\mathbf{a}, \tag{3.21}$$

together with $(\mathsf{S}_K)_\mathbf{a} := (\mathsf{P})_K$ for the vertex $\mathbf{a}$ of $\mathcal{T}_h$ lying inside $K \in \mathcal{T}_H$.

We finish this section by a remark on an alternative, still more precise potential reconstruction, that we will namely use for comparison in numerical experiments below:

Remark 3.11 (Piecewise quadratic potential reconstruction)**.** *Let $(\mathbf{u}_h, p_h)$ be given by Definition 3.3. Following [42, Section 4.1], let $\tilde{p}_h$ be a piecewise quadratic polynomial on the simplicial mesh $\mathcal{T}_h$ given by*

$$-\underline{\mathbf{K}}\nabla\tilde{p}_h|_\kappa = \mathbf{u}_h|_\kappa, \qquad \frac{(\tilde{p}_h, 1)_\kappa}{|\kappa|} = p_h|_\kappa \qquad \forall\kappa\in\mathcal{T}_h.$$

A typically more precise piecewise quadratic but computationally more demanding potential reconstruction $s_h \in \mathbb{P}_2(\mathcal{T}_h)H^1_0(\Omega)$ can be obtained by averaging the values of $\tilde{p}_h$ in all Lagrangian degrees of freedom, cf. [42, Section 4.2].

3.5 A simple guaranteed a posteriori error estimate

We now present our simple a posteriori error estimate. It is given for the error between the exact Darcy velocity $\mathbf{u} \in \mathbf{H}(\mathrm{div},\Omega)$ of (3.1)–(3.3) and the reconstruction $\mathbf{u}_h \in \mathbf{RTN}_0(\Omega)$ of Definition (3.3). This is similar to [6, 8] in that neither $\mathbf{u}$ nor $\mathbf{u}_h$ need not be known to give a computable estimate. An important difference, however, is that $\mathbf{u}_h$ can be computed if necessary following Definition 3.3 for our estimates; we will use this in the model problems in Section 4 below to rigorously verify their quality. Our main result is as follows:

Theorem 3.12 (A simple a posteriori error estimate for the steady Darcy flow)**.** *Let $\mathbf{u}$ be given by (3.2)–(3.3). For any polytopal discretization satisfying Assumption 3.1, let the flux $\mathbf{u}_h \in \mathbf{RTN}_0(\Omega)$ be reconstructed following Definition 3.3. Let the element matrices $\widehat{\mathbb{A}}_{\mathrm{MFE},K}$, $\widehat{\mathbb{S}}_{\mathrm{FE},K}$, and $\widehat{\mathbb{M}}_{\mathrm{FE},K}$ be respectively defined by (3.10), (3.16), and (3.18). Let finally the vectors S_K and $\mathsf{S}_K^{\mathrm{ext}}$ be given by (3.14), (3.15), or alternatively, for schemes of the form of Remark 3.2, by (3.21), (3.15). Then there holds*

$$\|\mathbf{u}-\mathbf{u}_h\|_{\underline{\mathbf{K}}^{-\frac12};L^2(\Omega)} \le \left\{\sum_{K\in\mathcal{T}_H}\eta_K^2\right\}^{\frac12}, \tag{3.22}$$

where

$$\eta_K^2 := (\mathsf{U}_K^{\mathrm{ext}})^{\mathrm{t}}\widehat{\mathbb{A}}_{\mathrm{MFE},K}\mathsf{U}_K^{\mathrm{ext}} + \mathsf{S}_K^{\mathrm{t}}\widehat{\mathbb{S}}_{\mathrm{FE},K}\mathsf{S}_K + 2(\mathsf{U}_K^{\mathrm{ext}})^{\mathrm{t}}\mathsf{S}_K^{\mathrm{ext}} - 2(\mathsf{F})_K|K|^{-1}1^{\mathrm{t}}\widehat{\mathbb{M}}_{\mathrm{FE},K}\mathsf{S}_K. \tag{3.23}$$

Proof. An argument of the type of the Prager–Synge equality [37] gives, for an arbitrary $s_h \in H^1_0(\Omega)$,

$$\|\mathbf{u}-\mathbf{u}_h\|_{\underline{\mathbf{K}}^{-\frac12};L^2(K)} \le \|\mathbf{u}_h + \underline{\mathbf{K}}\nabla s_h\|_{\underline{\mathbf{K}}^{-\frac12};L^2(K)},$$

see, e.g., [44, Theorem 6.1]. Note that the assumption that the source term f is elementwise constant is important here; then (3.4) of Assumption 3.1 together with Definition 3.3 imply $\nabla\cdot\mathbf{u}_h = f$. In the general case, a data oscillation term would appear. We now choose for s_h the fictitious potential reconstruction s_h

of Definition 3.7, continuous and piecewise affine with respect to $\mathcal{T}_h$ and given by the nodal values of the vector S. Developing elementwise, we obtain

$$\|\mathbf{u}_h + \underline{\mathbf{K}}\nabla s_h\|^2_{\underline{\mathbf{K}}^{-\frac{1}{2}};L^2(K)} = \|\mathbf{u}_h\|^2_{\underline{\mathbf{K}}^{-\frac{1}{2}};L^2(K)} + 2(\mathbf{u}_h, \nabla s_h)_K + \|\underline{\mathbf{K}}\nabla s_h\|^2_{\underline{\mathbf{K}}^{-\frac{1}{2}};L^2(K)}.$$

We now use Lemma 3.5 for the first term and (3.17) for the last one. For the middle term, recall first that the normal components of vector fields in $\mathbf{RTN}_0(\Omega)$ are constant on each face. Thus the Green theorem together with (3.15) and (3.19) give

$$(\mathbf{u}_h, \nabla s_h)_K = \langle \mathbf{u}_h{\cdot}\mathbf{n}, s_h\rangle_{\partial K} - (\nabla{\cdot}\mathbf{u}_h, s_h)_K = (\mathsf{U}_K^{\mathrm{ext}})^{\mathrm{t}}\mathsf{S}_K^{\mathrm{ext}} - (\mathsf{F})_K|K|^{-1}\mathsf{1}^{\mathrm{t}}\widehat{\mathbb{M}}_{\mathrm{FE},K}\mathsf{S}_K.$$

Thus the proof is finished. □

Note that the estimate of Theorem 3.12 takes a simple form of matrix-vector multiplication on each polytopal mesh element $K \in \mathcal{T}_H$ (recall that the element matrices $\widehat{\mathbb{A}}_{\mathrm{MFE},K}$, $\widehat{\mathbb{S}}_{\mathrm{FE},K}$, and $\widehat{\mathbb{M}}_{\mathrm{FE},K}$ can easily be constructed from the geometry of K and do not need the factual construction of the simplicial submesh $\mathcal{T}_K$), yet it delivers a guaranteed upper bound on the Darcy velocity error.

Remark 3.13 (Simplified a posteriori error estimates with the given element matrices $\widehat{\mathbb{A}}_K$)**.** *For any discretization of the form of Remark 3.2, the element matrix $\widehat{\mathbb{A}}_K$ is at disposal for any $K \in \mathcal{T}_H$. Thus, following Remark 3.6, it suggests itself to use in practice in (3.23) $\widehat{\mathbb{A}}_K$ instead of the element matrices $\widehat{\mathbb{A}}_{\mathrm{MFE},K}$ that one needs to construct by (3.10). Using in particular the approximation (3.12) (leading to "approximately less than or equal to" denoted by $\lesssim$) or the equality (3.13), this in particular gives*

$$\|\mathbf{u} - \mathbf{u}_h\|_{\underline{\mathbf{K}}^{-\frac{1}{2}};L^2(\Omega)} \lesssim \left\{\sum_{K\in\mathcal{T}_H} \eta_K^2\right\}^{\frac{1}{2}} \tag{3.24}$$

or

$$\|\mathbf{u} - \tilde{\mathbf{u}}_h\|_{\underline{\mathbf{K}}^{-\frac{1}{2}};L^2(\Omega)} \leq \left\{\sum_{K\in\mathcal{T}_H} \eta_K^2\right\}^{\frac{1}{2}}, \tag{3.25}$$

where

$$\eta_K^2 := (\mathsf{U}_K^{\mathrm{ext}})^{\mathrm{t}}\widehat{\mathbb{A}}_K\mathsf{U}_K^{\mathrm{ext}} + \mathsf{S}_K^{\mathrm{t}}\widehat{\mathbb{S}}_{\mathrm{FE},K}\mathsf{S}_K + 2(\mathsf{U}_K^{\mathrm{ext}})^{\mathrm{t}}\mathsf{S}_K^{\mathrm{ext}} - 2(\mathsf{F})_K|K|^{-1}\mathsf{1}^{\mathrm{t}}\widehat{\mathbb{M}}_{\mathrm{FE},K}\mathsf{S}_K. \tag{3.26}$$

In the numerical experiments in Section 4 below, inequality (3.24) actually holds with $\leq$ and results very close to Theorem 3.12 are observed.

4 Numerical experiments: single-phase Darcy flow

The purpose of this section is to numerically illustrate the performance of the estimators of Theorem 3.12, as well as the simplified estimate (3.24) of Remark 3.13. The test is taken from [34], where a collection of two-dimensional elliptic problems for testing adaptive grid refinement algorithms is proposed. We approximate $-\Delta p = f$ on the space domain $\Omega = (0,1)^2$ with Dirichlet boundary conditions prescribed by the analytic solution $2^{4\alpha}x^\alpha(1-x)^\alpha y^\alpha(1-y)^\alpha$ with $\alpha = 200$, see Figure 3.

The mesh $\mathcal{T}_H$ consists of general polygonal elements, with the fictitious triangular submesh $\mathcal{T}_h$ shown in Figure 4. We consider the hybrid finite volume (HFV) discretization (Droniou *et al.* [23, Section 2.2]), taking the form (3.5) with the matrix $\mathbb{A}$ formed by local element matrices $\widehat{\mathbb{A}}_K$. We compare three versions of a posteriori error estimates: a) the estimators η_K in (3.23) of Theorem 3.12 are replaced by the expression $\left\|\underline{\mathbf{K}}^{-\frac{1}{2}}\mathbf{u}_h + \underline{\mathbf{K}}^{\frac{1}{2}}\nabla s_h\right\|_K$, where $\mathbf{u}_h|_K \in \mathbf{V}^K_{h,\mathrm{N}}$ is given in Definition 3.3 and $s_h \in \mathbb{P}_2(\mathcal{T}_h)\cap H^1_0(\Omega)$ is described in Remark 3.11 (called triangular MFE estimate); b) Theorem 3.12 is used, with the estimators η_K evaluated via the matrix form (3.23), relying on the element matrices $\widehat{\mathbb{A}}_{\mathrm{MFE},K}$, $\widehat{\mathbb{S}}_{\mathrm{FE},K}$, and $\widehat{\mathbb{M}}_{\mathrm{FE},K}$ of respectively (3.10), (3.16), and (3.18) (called polygonal MFE estimate); c) Remark 3.13 is employed, with the bound (3.24) and the estimators of (3.26) using the element matrix $\widehat{\mathbb{A}}_K$ of the HFV scheme that is already available (called polygonal HFV estimate).

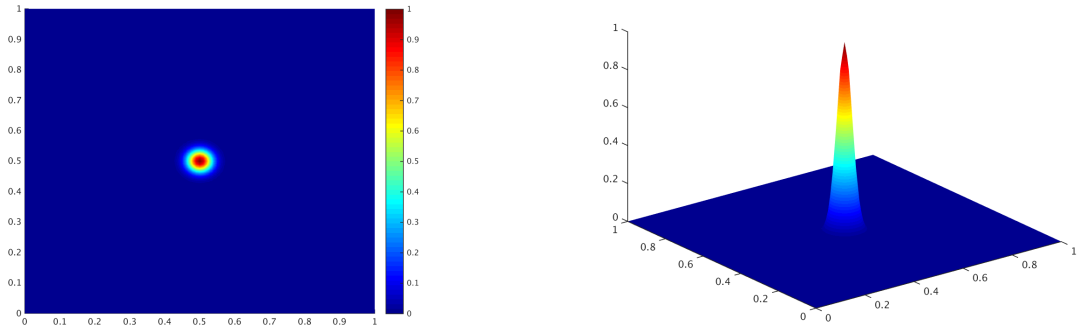

Figure 3: The solution of the analytic problem with $\alpha = 200$

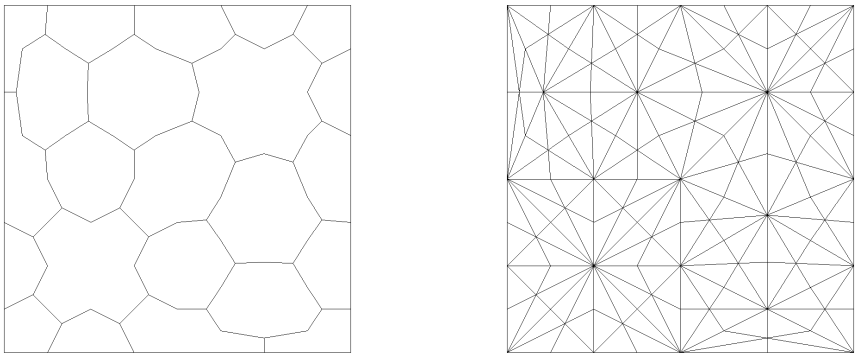

Figure 4: An example of a polygonal mesh $\mathcal{T}_H$ and the corresponding triangular submesh $\mathcal{T}_h$

Note that if the mixed finite element method on polygonal meshes of [46, Theorem 7.2] is used instead of the HFV discretization, the first procedure is, following [46, Remark 7.3], fully equivalent to solving the problem (3.1) directly on the simplicial mesh $\mathcal{T}_h$ by the lowest-order Raviart–Thomas–Nédélec mixed finite element method and applying the a posteriori error estimates of [42]. It serves here as a sort of a reference a posteriori error estimate. The second procedure only uses the piecewise affine potential reconstruction s_h of Definition 3.7, which allows for the simple matrix form (3.23) of the estimators. The last procedure is definitely the easiest choice in practice, where only the already available element matrices $\widehat{\mathbb{A}}_K$ are used and there is no need to construct the mixed finite element matrices $\widehat{\mathbb{A}}_{\mathrm{MFE},K}$ via (3.10).

In Figure 5 we compare the actual and predicted error distributions. Obviously, the energy error and the rigorous triangular MFE estimate distributions match perfectly. The polygonal MFE estimate and the polygonal HFV estimates give similar results and match also well with the energy error. We depict in Figure 6 the error and estimates as a function of the total number of unknowns and the corresponding effectivity indices for a uniform mesh refinement. All the three estimators behave in a similar way, with a slight advantage for the triangular MFE estimate. The graphs confirm in particular that replacing the mixed finite element matrix $\widehat{\mathbb{A}}_{\mathrm{MFE},K}$ by $\widehat{\mathbb{A}}_K$ has a very small influence.

Figure 7 shows the results for adaptive mesh refinement, achieved by using the local distribution of the predicted error as an indicator to refine only the cells of the mesh where the error is important. We observe quasi-identical values of the polygonal MFE and polygonal HFV estimates; consequently, we obtain the same number of unknowns at each step of adaptivity and almost identical final energy error for these two estimators. The left part of Figure 7 displays the results where we present the estimators and two energy errors, one resulting with adaptivity based on the polygonal estimates and another with adaptivity based on the triangular MFE estimates. Finally, adaptivity leads to both smaller error and better effectivity indices

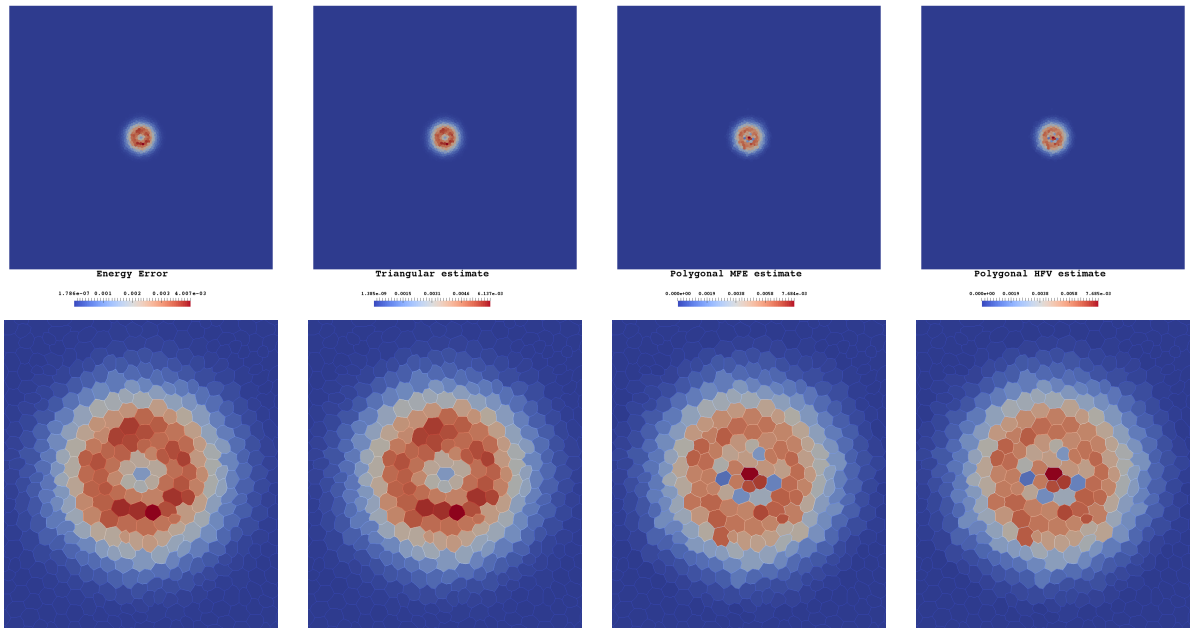

(a) Energy error (b) Triangular MFE estimate (c) Polygonal MFE estimate (d) Polygonal HFV estimate

Figure 5: Actual and estimated error distributions, entire domain (*top*) and center zoom (*bottom*)

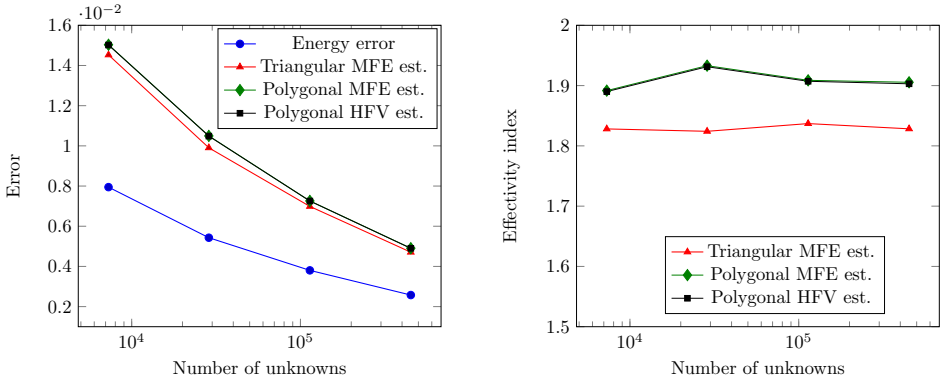

Figure 6: Error and estimators (left) and effectivity indices (right), uniform mesh refinement

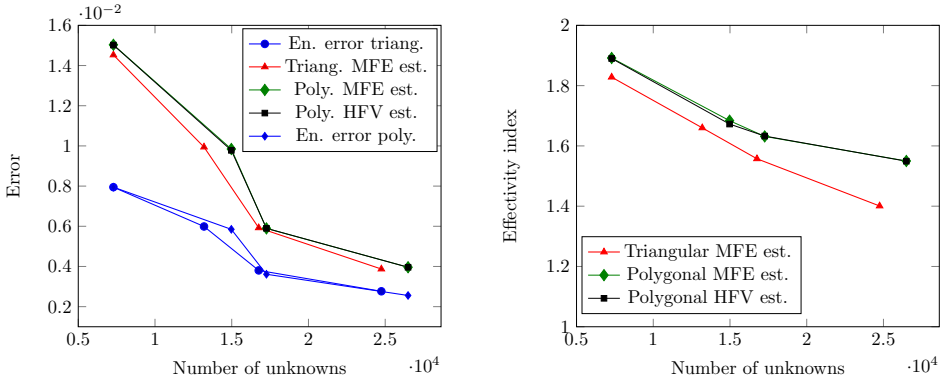

Figure 7: Error and estimators (left) and effectivity indices (right), adaptive mesh refinement

in comparison with uniform mesh refinement.

5 A coupled unsteady nonlinear problem

In this section, the methodology derived in Section 3 is applied to polytopal discretizations of multiphase Darcy flows in porous media. An abstract framework for a posteriori estimates is already developed for two-phase flow in [45, 15], for multiphase compositional flow in [20], and for thermal multiphase compositional flow in [21]. However, these works do not handle general polytopal meshes often encountered in practice and do not address the question of as cheap as possible form of the estimates. In the following, we describe briefly the multiphase model, discuss its discretization by an implicit finite volume scheme, the linearization by the Newton methods, and the algebraic solution of the arising linear system. We also explain the required fictitious flux reconstructions and finally develop our simple a posteriori error estimate distinguishing different error components. By decomposing the estimators into the space, time, linearization, and algebraic error components, we can formulate criteria for stopping the iterative algebraic solver and the iterative linearization solver when the corresponding error components do not affect significantly the overall error. Moreover, the spatial and temporal error components can be balanced respectively by time step and space mesh adaptation. In particular, denote by $\eta_{\mathrm{sp,t}}^{n,k,i}$, $\eta_{\mathrm{tm,t}}^{n,k,i}$, $\eta_{\mathrm{lin,t}}^{n,k,i}$, and $\eta_{\mathrm{alg,t}}^{n,k,i}$ respectively the total spatial, temporal, linearization, and algebraic estimators, on time step n, linearization step k, and algebraic solvers step i. Let $\gamma_{\mathrm{lin}}, \gamma_{\mathrm{alg}} \in (0,1)$ and $\Gamma_{\mathrm{tm}} > \gamma_{\mathrm{tm}} > 0$ be user-given fixed parameters. Similarly, fix the margins of cells to refine ζ_{ref} and to derefine ζ_{deref}, $0 < \zeta_{\mathrm{deref}} < \zeta_{\mathrm{ref}} < 1$. Following [26, 45, 15, 20] and the references therein, we derive in this section simple estimators to run the following *fully adaptive algorithm*:

Algorithm 5.1 (Adaptive algorithm with time and space mesh refinement and adaptive stopping criteria)**.**

Set $n := 0$.
while $t^n \le t_{\mathrm{F}}$ **do** {Time loop}
  Set $n := n + 1$.
  loop {Spatial and temporal errors balancing loop}
    Set $k := 0$.
    loop {Standard Newton linearization loop}
      Set $k := k + 1$.
      Set up the linear system.
      Set $i := 0$.
      loop {Algebraic solver loop}
        Perform a step of the iterative algebraic solver and set $i := i + 1$.
        Evaluate the different estimators.
        Terminate the algebraic solver loop if: $\eta_{\mathrm{alg,t}}^{n,k,i} \le \gamma_{\mathrm{alg}}\big(\eta_{\mathrm{sp,t}}^{n,k,i}\big)$.
      end loop
      Terminate the Newton linearization loop if: $\eta_{\mathrm{lin,t}}^{n,k,i} \le \gamma_{\mathrm{lin}}\big(\eta_{\mathrm{sp,t}}^{n,k,i}\big)$.
    end loop
    Terminate the spatial and temporal errors balancing loop if

$$\eta_{\mathrm{sp},K,\mathrm{t}}^{n,k,i} \ge \zeta_{\mathrm{ref}} \max_{K' \in \mathcal{T}_H^n} \big\{\eta_{\mathrm{sp},K',\mathrm{t}}^{n,k,i}\big\} \qquad \forall K \in \mathcal{T}_H^n$$

$$\gamma_{\mathrm{tm}}\big(\eta_{\mathrm{sp,t}}^{n,k,i}\big) \le \eta_{\mathrm{tm,t}}^{n,k,i} \le \Gamma_{\mathrm{tm}}\big(\eta_{\mathrm{sp,t}}^{n,k,i}\big);$$

    else
    Refine the cells $K \in \mathcal{T}_H^n$ such that $\eta_{\mathrm{sp},K,\mathrm{t}}^{n,k,i} \ge \zeta_{\mathrm{ref}} \max_{K' \in \mathcal{T}_H^n} \big\{\eta_{\mathrm{sp},K',\mathrm{t}}^{n,k,i}\big\}$.
    Derefine the cells $K \in \mathcal{T}_H^n$ such that $\eta_{\mathrm{sp},K,\mathrm{t}}^{n,k,i} \le \zeta_{\mathrm{deref}} \max_{K' \in \mathcal{T}_H^n} \big\{\eta_{\mathrm{sp},K',\mathrm{t}}^{n,k,i}\big\}$.
    Refine the time step if $\eta_{\mathrm{tm,t}}^{n,k,i} > \Gamma_{\mathrm{tm}}\big(\eta_{\mathrm{sp,t}}^{n,k,i}\big)$, derefine the time step if $\gamma_{\mathrm{tm}}\big(\eta_{\mathrm{sp,t}}^{n,k,i}\big) > \eta_{\mathrm{tm,t}}^{n,k,i}$.
  end loop
  Update data.
end while

5.1 Multiphase Darcy flow

We consider the generalization of Coats' formulation [18] of multiphase Darcy flow models to an arbitrary number of phases by [29]. The same formulation has already been used in [20], so we only give a concise presentation. Let $\mathcal{P} = \{p\}$ be the set of *phases*, $\mathcal{C} = \{c\}$ the set of *components*, and, for a given phase $p \in \mathcal{P}$, let $\mathcal{C}_p \subset \mathcal{C}$ be the set of its components. S_p then denotes the *saturation* of the phase p and $C_{p,c}$ the *molar fraction* of the component c in the phase p. For a given component $c \in \mathcal{C}$, denote by $\mathcal{P}_c$ the set of the phases which contain c.

We denote by P the *reference pressure* such that the *phase pressures* P_p, $p \in \mathcal{P}$, are expressed as

$$P_p := P + P_{c_p}(S_p), \tag{5.1}$$

where P_{c_p} is a given generalized capillary pressure function. We collect the unknowns of the model in the vector $\boldsymbol{\mathcal{X}} := (P, (S_p)_{p\in\mathcal{P}}, (C_{p,c})_{p\in\mathcal{P}, c\in\mathcal{C}_p})$. We denote by ϕ the porosity of the medium and by $\underline{\mathbf{K}}$ the permeability tensor. For a phase $p \in \mathcal{P}$, $k_{r,p}$ is the relative permeability, μ_p is the dynamic viscosity, ζ_p is the molar density, ρ_p is the mass density, and ν_p is the mobility given by $\nu_p := \zeta_p \frac{k_{r,p}}{\mu_p}$; for simplicity, we suppose here that only $k_{r,p}$ (and consequently ν_p) can be functions of the unknown saturations S_p, the other data being given as constants. More general cases can be treated as in [20].

The system of governing equations is given by

$$\partial_t \mathcal{L}_c + \nabla\cdot\boldsymbol{\Phi}_c = q_c, \qquad \forall c \in \mathcal{C}, \tag{5.2}$$

where $q_c \in L^2((0, t_F); L^2(\Omega))$ denotes a *source or sink* and $\mathcal{L}_c$ is the *amount* (in moles) of component c per unit volume,

$$\mathcal{L}_c = \phi \sum_{p\in\mathcal{P}_c} \zeta_p S_p C_{p,c}. \tag{5.3}$$

For simplicity, q_c is supposed to be piecewise constant on the space-time mesh; this is the case for the numerical tests chosen in Section 6 below. Additionally, in (5.2), for each $c \in \mathcal{C}$, the *component flux* $\boldsymbol{\Phi}_c$ has the following expression:

$$\boldsymbol{\Phi}_c := \sum_{p\in\mathcal{P}_c} \boldsymbol{\Phi}_{p,c}, \qquad \boldsymbol{\Phi}_{p,c} = \boldsymbol{\Phi}_{p,c}(\boldsymbol{\mathcal{X}}) := \nu_p C_{p,c} \boldsymbol{v}_p(P_p), \tag{5.4}$$

and for all $p \in \mathcal{P}$, $\boldsymbol{v}_p(P_p)$ represents the average *phase velocity* given by Darcy's law,

$$\boldsymbol{v}_p(P_p) = -\underline{\mathbf{K}}\,(\nabla P_p + \rho_p g \nabla z)\,. \tag{5.5}$$

Here g is the gravitation acceleration constant. We assume that no-flow boundary conditions are prescribed for all the component fluxes,

$$\boldsymbol{\Phi}_c\cdot\boldsymbol{n}_\Omega = 0 \qquad \text{on } \partial\Omega \times (0, t_F) \qquad \forall c \in \mathcal{C}, \tag{5.6}$$

where $\partial\Omega$ denotes the boundary of Ω and $\boldsymbol{n}_\Omega$ its unit outward normal. At $t = 0$ we prescribe the *initial amount* of each component,

$$\mathcal{L}_c(\cdot, 0) = \mathcal{L}_c^0 \qquad \forall c \in \mathcal{C}. \tag{5.7}$$

The previous PDEs is supplemented by a system of algebraic equations imposing the volume conservation:

$$\sum_{p\in\mathcal{P}} S_p = 1, \tag{5.8}$$

the conservation of the quantity of matter:

$$\sum_{c\in\mathcal{C}_p} C_{p,c} = 1 \qquad \forall p \in \mathcal{P}, \tag{5.9}$$

and local thermodynamic equilibrium expressed by

$$\sum_{c\in\mathcal{C}} (N_{\mathcal{P}_c} - 1) = \sum_{p\in\mathcal{P}} N_{\mathcal{C}_p} - N_{\mathcal{C}} \tag{5.10}$$

equalities of fugacities, see [20] for more details.

5.2 Finite volume discretization on a polytopal mesh

To discretize our model, we choose a fully implicit numerical scheme based on phase-upwind and multi-point flux approximation L-method, see [1]. This method, in the steady linear case, fits our Assumption 3.1 but is not of the form of Remark 3.2. In order to define this numerical scheme, we start by giving some notations for the space-time mesh. In addition to Section 2 for the space mesh, we let $(\tau_n)_{1\le n\le N}$ denote a sequence of positive real numbers corresponding to the discrete time steps such that $t_{\rm F}=\sum_{n=1}^{N}\tau_n$. We consider the discrete times $(t^n)_{0\le n\le N}$ such that $t^0:=0$ and, for $1\le n\le N$, $t^n:=\sum_{i=1}^{n}\tau_i$; then we define the time intervals $I_n:=(t^{n-1},t^n)$.

Let $(\mathcal{T}_H^n)_{0\le n\le N}$ denote a family of meshes of the space domain Ω defined in the sense of Section 2. For all $0\le n\le N$ we define $\mathcal{E}_H^n$, $\mathcal{E}_h^n$, $\mathcal{E}_{H,h}^n$, $\mathcal{E}_{K,h}^{n,\rm ext}$, and $\mathcal{E}_{K,h}^{n,\rm int}$ similarly to Section 2. The key idea of the MPFA L-method is to express fluxes as a linear combination of cell unknowns, using one value per cell. For all $1\le n\le N$, we let $\boldsymbol{\mathcal{X}}_{\mathcal{T}_H}^n:=(\boldsymbol{\mathcal{X}}_K^n)_{K\in\mathcal{T}_H^n}$, with $\boldsymbol{\mathcal{X}}_K^n:=(P_K^n,(S_{p,K}^n)_{p\in\mathcal{P}},(C_{p,c,K}^n)_{p\in\mathcal{P},c\in\mathcal{C}_p})$. System 5.2 is then discretized as follows: for all $1\le n\le N$, $K\in\mathcal{T}_H^n$, and each $c\in\mathcal{C}$, we require

$$\frac{|K|}{\tau^n}\big(\mathcal{L}_{c,K}(\boldsymbol{\mathcal{X}}_K^n)-\mathcal{L}_{c,K}(\boldsymbol{\mathcal{X}}_K^{n-1})\big)+\sum_{\sigma\in\mathcal{E}_K\cap\mathcal{E}_H^{\rm int}}\mathcal{F}_{c,K,\sigma}(\boldsymbol{\mathcal{X}}_{\mathcal{T}_H}^n)=|K|q_{c,K}^n,\qquad\forall c\in\mathcal{C},\ \forall K\in\mathcal{T}_H^n. \tag{5.11}$$

This equation expresses the mass balance for the element K. Here $q_{c,K}^n$ is the value of q_c on element K and time interval I_n; recall also that $|K|$ stands for the Lebesgue measure of the element K. For each component $c\in\mathcal{C}$, its total flux across the face σ results from the sum of the corresponding fluxes for each phase $p\in\mathcal{P}_c$, i.e., for all $K\in\mathcal{T}_H^n$ and all $\sigma\in\mathcal{E}_K\cap\mathcal{E}_H^{\rm int}$ with $\sigma=\partial K\cap\partial K'$,

$$\mathcal{F}_{c,K,\sigma}(\boldsymbol{\mathcal{X}}_{\mathcal{T}_H}^n):=\sum_{p\in\mathcal{P}_c}\nu_{p,K_p^\uparrow}^n C_{p,c,K_p^\uparrow}^n\mathcal{F}_{p,K,\sigma}(\boldsymbol{\mathcal{X}}_{\mathcal{T}_H}^n),\qquad K_p^\uparrow:=\begin{cases}K & \text{if } \mathcal{F}_{p,K,\sigma}(\boldsymbol{\mathcal{X}}_{\mathcal{T}_H}^n)\ge 0,\\ K' & \text{otherwise,}\end{cases} \tag{5.12}$$

and with $C_{p,c,K_p^\uparrow}^n$ and $\nu_{p,K_p^\uparrow}^n$ denoting, respectively, the upstream molar fraction and upstream mobility. Finally,

$$\mathcal{L}_{c,K}(\boldsymbol{\mathcal{X}}_K^n):=\phi_K\sum_{p\in\mathcal{P}_c}\zeta_{p,K}^n S_{p,K}^n C_{p,c,K}^n.$$

In (5.12), we have introduced the multi-point finite volume approximation of the normal component of the average phase velocity on face σ given by

$$\mathcal{F}_{p,K,\sigma}(\boldsymbol{\mathcal{X}}_{\mathcal{T}_H}^n):=\mathcal{F}_{p,K,\sigma}(\{\boldsymbol{\mathcal{X}}_{K'}^n\}_{K'\in\mathcal{S}_\sigma^L}):=\sum_{K'\in\mathcal{S}_\sigma^L}\tau_{K'}^\sigma(P_{p,K'}^n+\rho_{p,\sigma}^n g z_{K'}), \tag{5.13}$$

where, for all $\sigma\in\mathcal{E}_K\cap\mathcal{E}_H^{\rm int}$, $\mathcal{S}_\sigma^L$ is a flux L-stencil $\mathcal{S}_\sigma^L\in\mathcal{T}_H$, for all $K\in\mathcal{S}_\sigma^L$, $\tau_K^\sigma\in\mathbb{R}$ is the transmissibility coefficient of the face σ, and

$$P_{p,K}^n:=P_K^n+P_{{\rm c}_p}(S_{p,K}^n)$$

following (5.1). Details about choosing the proper L-stencil and computing the corresponding transmissibility coefficients can be found in [1]. Finally, boundary fluxes are set to zero to account for the homogeneous natural boundary conditions.

5.3 Linearization and algebraic system solution

At this stage, we need to solve, at each time step, the system of nonlinear algebraic equations resulting from the discretization (5.11). First, for all times $1\le n\le N$, we apply the *Newton linearization algorithm* generating, for $\boldsymbol{\mathcal{X}}_{\mathcal{T}_H}^{n,0}$ fixed, a sequence $(\boldsymbol{\mathcal{X}}_{\mathcal{T}_H}^{n,k})_{k\ge1}$ with $\boldsymbol{\mathcal{X}}_{\mathcal{T}_H}^{n,k}$ solution to the following *system of linear algebraic equations*: for all components $c\in\mathcal{C}$ and all mesh elements $K\in\mathcal{T}_H^n$,

$$\sum_{K'\in\mathcal{T}_H^n}\frac{\partial\mathcal{R}_{c,K}}{\partial\boldsymbol{\mathcal{X}}_{K'}^n}(\boldsymbol{\mathcal{X}}_{\mathcal{T}_H}^{n,k-1})\cdot(\boldsymbol{\mathcal{X}}_{K'}^{n,k}-\boldsymbol{\mathcal{X}}_{K'}^{n,k-1})+\mathcal{R}_{c,K}(\boldsymbol{\mathcal{X}}_{\mathcal{T}_H}^{n,k-1})=0, \tag{5.14}$$

with, for all $c \in \mathcal{C}$ and $K \in \mathcal{T}_H^n$,

$$\mathcal{R}_{c,K}(\boldsymbol{\mathcal{X}}_{\mathcal{T}_H}^n) := \frac{|K|}{\tau^n}\big(\mathcal{L}_{c,K}(\boldsymbol{\mathcal{X}}_K^n) - \mathcal{L}_{c,K}(\boldsymbol{\mathcal{X}}_K^{n-1})\big) + \sum_{\sigma\in\mathcal{E}_K\cap\mathcal{E}_H^{\rm int}} \mathcal{F}_{c,K,\sigma}(\boldsymbol{\mathcal{X}}_{\mathcal{T}_H}^n) - |K| q_{c,K}^n.$$

Second, for time $1 \le n \le N$, and a given Newton iteration $k \ge 1$, to approximate the solution of the system (5.14), we use an *iterative algebraic solver* generating, for $\boldsymbol{\mathcal{X}}_{\mathcal{T}_H}^{n,k,0}$ fixed, a sequence $(\boldsymbol{\mathcal{X}}_{\mathcal{T}_H}^{n,k,i})_{i\ge1}$ solving (5.14) up to the residuals, given for all $c \in \mathcal{C}$ and all $K \in \mathcal{T}_H^n$ by

$$\mathcal{R}_{c,K}^{n,k,i} := \frac{|K|}{\tau^n}\Big(\mathcal{L}_{c,K}(\boldsymbol{\mathcal{X}}_K^{n,k-1}) + \mathcal{L}_{c,K}^{n,k,i} - \mathcal{L}_{c,K}(\boldsymbol{\mathcal{X}}_K^{n-1})\Big) + \sum_{\sigma\in\mathcal{E}_K\cap\mathcal{E}_H^{\rm int}} \mathcal{F}_{c,K,\sigma}^{n,k,i} - |K| q_{c,K}^n, \tag{5.15}$$

where

$$\mathcal{L}_{c,K}^{n,k,i} := \frac{\partial \mathcal{L}_{c,K}}{\partial \boldsymbol{\mathcal{X}}_K^n}(\boldsymbol{\mathcal{X}}_K^{n,k-1}) \cdot (\boldsymbol{\mathcal{X}}_K^{n,k} - \boldsymbol{\mathcal{X}}_K^{n,k-1})$$

and where $\mathcal{F}_{c,K,\sigma}^{n,k,i}$ are the linearized component fluxes given by

$$\mathcal{F}_{c,K,\sigma}^{n,k,i} := \sum_{p\in\mathcal{P}_c}\left[\mathcal{F}_{p,c,K,\sigma}(\boldsymbol{\mathcal{X}}_{\mathcal{T}_H}^{n,k-1}) + \sum_{K'\in\mathcal{T}_H^n} \frac{\partial \mathcal{F}_{p,c,K,\sigma}}{\partial \boldsymbol{\mathcal{X}}_{K'}^n}(\boldsymbol{\mathcal{X}}_{\mathcal{T}_H}^{n,k-1}) \cdot (\boldsymbol{\mathcal{X}}_{K'}^{n,k,i} - \boldsymbol{\mathcal{X}}_{K'}^{n,k-1})\right], \tag{5.16}$$

with

$$\mathcal{F}_{p,c,K,\sigma}(\boldsymbol{\mathcal{X}}_{\mathcal{T}_H}^{n,k-1}) := \nu_{p,K_p^\uparrow}^{n,k-1} C_{p,c,K_p^\uparrow}^{n,k-1} \mathcal{F}_{p,K,\sigma}(\boldsymbol{\mathcal{X}}_{\mathcal{T}_H}^{n,k-1}).$$

Above, we use that we have supposed the accumulation term $\mathcal{L}_c$ to be linear; general nonlinear accumulation terms can be treated following [20].

5.4 Fictitious flux reconstructions

Following Section 3.3, we now define an equivalent of $\mathbf{u}_h$ of Definition 3.3. Here again, it is only needed to define the approximate solution but not for the a posteriori error estimators, so that it is not to be constructed in practical calculations. In what follows, as we will systematically use the convention (3.7) (without change of the notation) to define the fluxes of the simplicial submesh faces in case they subdivide the original polytopal faces.

Let a time step $1 \le n \le N$, a Newton linearization iteration $k \ge 1$, and an algebraic solver iteration $i \ge 1$ be fixed. For all phases $p \in \mathcal{P}$ and all $K \in \mathcal{T}_H^n$, define $\mathbf{u}_{p,h}^{n,k,i}|_K \in \mathbf{RTN}_0(K)$ such that

$$\langle \mathbf{u}_{p,h}^{n,k,i}\cdot\boldsymbol{n}_K, 1\rangle_\sigma := \sum_{K'\in\mathcal{S}_\sigma^L} \tau_{K'}^\sigma P_{p,K'}^{n,k,i}, \qquad \forall \sigma \in \mathcal{E}_{K,h}^{n,\rm ext}, \tag{5.17}$$

with $\mathbf{u}_{p,h}^{n,k,i}\cdot\boldsymbol{n}_\Omega = 0$ on $\partial\Omega$ coherently with the homogeneous boundary condition. Similarly, for all components $c \in \mathcal{C}$ and all $K \in \mathcal{T}_H^n$, we define $\boldsymbol{\Phi}_{c,h}^{n,k,i}|_K \in \mathbf{RTN}_0(K)$ such that

$$\langle \boldsymbol{\Phi}_{c,h}^{n,k,i}\cdot\boldsymbol{n}_K, 1\rangle_\sigma := \sum_{p\in\mathcal{P}_c} \nu_{p,K}^{n,k,i} C_{p,c,K}^{n,k,i} \mathcal{F}_{p,K,\sigma}(\boldsymbol{\mathcal{X}}_{\mathcal{T}_H}^{n,k,i}), \qquad \forall \sigma \in \mathcal{E}_{K,h}^{n,\rm ext}, \tag{5.18}$$

with $\mathcal{F}_{p,K,\sigma}$ defined by (5.13), and we set $\boldsymbol{\Phi}_{c,h}^{n,k,i}\cdot\boldsymbol{n}_\Omega = 0$ on $\partial\Omega$. The other degrees of freedom are then defined via a minimization solve as in Definition 3.3.

5.5 Error via dual norm of the residual and potential nonconformity

Suppose that a weak solution can be defined as in [20, Assumption 3.1]. Let $X := L^2(0, t_{\rm F}; H^1(\Omega))$ and set

$$\|\varphi\|_X^2 := \sum_{n=1}^N \int_{I_n} \sum_{K\in\mathcal{T}_H^n} \|\varphi\|_{X,K}^2 \,\mathrm{d}t, \qquad \|\varphi\|_{X,K}^2 := h_K^{-2}\|\varphi\|_{L^2(K)}^2 + \left\|\underline{\mathbf{K}}^{\frac12}\nabla\varphi\right\|_{L^2(K)}^2.$$

We also need to define $\mathcal{L}_{c,h\tau}^{n,k,i} \in H^1(0,t_\mathrm{F};L^2(\Omega))$ as piecewise affine and continuous in time, given by the values $\mathcal{L}_{c,K}(\boldsymbol{\mathcal{X}}_K^{n,k,i})$ at times t^n, $0 \le n \le N$. Similarly, let $\mathbf{u}_{p,h\tau}^{n,k,i}$ and $\boldsymbol{\Phi}_{c,h\tau}^{n,k,i}$ be piecewise affine and continuous in time, given respectively by $\mathbf{u}_{p,h}^{n,k,i}$ and $\boldsymbol{\Phi}_{c,h}^{n,k,i}$ of (5.17)–(5.18) at times t^n. Then the distance of the current approximate solution to the exact solution can be evaluated as in [20, Section 3.3] via

$$\mathcal{N}^{n,k,i} = \mathcal{N}^{n,k,i}(\boldsymbol{\mathcal{X}}_{\mathcal{T}_H}^{n,k,i}) := \left\{ \sum_{c\in\mathcal{C}} \left(\mathcal{N}_c^{n,k,i}\right)^2 \right\}^{\frac{1}{2}} + \left\{ \sum_{p\in\mathcal{P}} \left(\mathcal{N}_p^{n,k,i}\right)^2 \right\}^{\frac{1}{2}}, \tag{5.19a}$$

where

$$\mathcal{N}_c^{n,k,i} := \sup_{\varphi\in X, \|\varphi\|_X=1} \int_0^{t_\mathrm{F}} \left\{ (\partial_t \mathcal{L}_c - \partial_t \mathcal{L}_{c,h\tau}^{n,k,i}, \varphi)(t) - \left(\boldsymbol{\Phi}_c - \boldsymbol{\Phi}_{c,h\tau}^{n,k,i}, \nabla\varphi \right)(t) \right\} \mathrm{d}t, \tag{5.19b}$$

and

$$\mathcal{N}_p^{n,k,i} := \inf_{\delta_p\in X} \left\{ \sum_{c\in\mathcal{C}_p} \int_0^{t_\mathrm{F}} \left\{ \sum_{K\in\mathcal{T}_H^n} \left(\nu_{p,K}^{n,k,i} C_{p,c,K}^{n,k,i} \right)^2 \left\| \mathbf{u}_{p,h\tau}^{n,k,i} - \underline{\mathbf{K}} \nabla \delta_p \right\|_{\underline{\mathbf{K}}^{-\frac{1}{2}};L^2(K)}^2 \right\} \mathrm{d}t \right\}^{\frac{1}{2}}. \tag{5.19c}$$

The first term (5.19b) is the dual norm of the residual of the weak formulation for each component. The second term (5.19c) then evaluates the nonconformity in the primal variables phase pressures.

5.6 Simple a posteriori error estimate distinguishing the different error components

We now extend the a posteriori estimates proposed in [20] to polytopal meshes and derive their simple form only relying on local matrix-vector multiplications. We rely on the following finite volume face fluxes associated with the polytopal mesh elements $K \in \mathcal{T}_H^n$ and their faces $\sigma \in \mathcal{E}_{K,h}^{n,\mathrm{ext}}$ not lying on the boundary of Ω, for all components $c \in \mathcal{C}$, time levels $n \ge 1$ and times $t \in I_n$, linearization steps $k \ge 1$, and algebraic iterations $i \ge 1$:

$$(\mathsf{U}_{K,p}^{n,k,i})_\sigma := \frac{t-t^{n-1}}{\tau^n} \nu_{p,K}^{n,k,i} C_{p,c,K}^{n,k,i} \sum_{K'\in\mathcal{S}_\sigma^L} \tau_{K'}^\sigma P_{p,K'}^{n,k,i} + \frac{t^n-t}{\tau^n} \nu_{p,K}^{n-1} C_{p,c,K}^{n-1} \sum_{K'\in\mathcal{S}_\sigma^L} \tau_{K'}^\sigma P_{p,K'}^{n-1}, \tag{5.20a}$$

$$(\mathsf{U}_{\mathrm{upw},K,c}^{n,k,i})_\sigma := \mathcal{F}_{c,K,\sigma}(\boldsymbol{\mathcal{X}}_{\mathcal{T}_H}^{n,k,i}) - \sum_{p\in\mathcal{P}_c} \nu_{p,K}^{n,k,i} C_{p,c,K}^{n,k,i} \mathcal{F}_{p,K,\sigma}(\boldsymbol{\mathcal{X}}_{\mathcal{T}_H}^{n,k,i}), \tag{5.20b}$$

$$(\mathsf{U}_{\mathrm{tm},K,c}^{n,k,i})_\sigma := \frac{t^n-t}{\tau^n} \sum_{p\in\mathcal{P}_c} \left[\nu_{p,K}^{n,k,i} C_{p,c,K}^{n,k,i} \mathcal{F}_{p,K,\sigma}(\boldsymbol{\mathcal{X}}_{\mathcal{T}_H}^{n,k,i}) - \nu_{p,K}^{n-1} C_{p,c,K}^{n-1} \mathcal{F}_{p,K,\sigma}(\boldsymbol{\mathcal{X}}_{\mathcal{T}_H}^{n-1}) \right], \tag{5.20c}$$

$$(\mathsf{U}_{\mathrm{lin},K,c}^{n,k,i})_\sigma := \mathcal{F}_{c,K,\sigma}^{n,k,i} - \mathcal{F}_{c,K,\sigma}(\boldsymbol{\mathcal{X}}_{\mathcal{T}_H}^{n,k,i}), \tag{5.20d}$$

$$(\mathsf{U}_{\mathrm{alg},K,c}^{n,k,i})_\sigma := \mathcal{F}_{c,K,\sigma}^{n,k,i+j} - \mathcal{F}_{c,K,\sigma}^{n,k,i}; \tag{5.20e}$$

we set all these normal fluxes to zero for all faces located on the boundary of Ω in accordance with the Neumann boundary condition (5.6) and define the local vectors as $\mathsf{U}_{\mathrm{x},K,c}^{n,k,i} := \{(\mathsf{U}_{\mathrm{x},K,c}^{n,k,i})_\sigma\}_{\sigma\in\mathcal{E}_K}$, $\mathrm{x} = \mathrm{upw}, \mathrm{tm}, \mathrm{lin}, \mathrm{alg}$, and similarly for $(\mathsf{U}_{K,p}^{n,k,i})_\sigma$.

We also need to define the phase pressure reconstructions $\mathsf{S}_{K,p}^{n,k,i}$ and $\mathsf{S}_{K,p}^{\mathrm{ext},n,k,i}$. Similarly to the steady linear model in Section 3.4, we use directly the cells pressure values as in Definition 3.7. Here the building blocks are the phase pressure values obtained from the finite volume scheme, the current $P_{p,K}^{n,k,i}$ and the previous time step $P_{p,K}^{n-1}$, that we combine for each time $t \in I_n$ to

$$\frac{t-t^{n-1}}{\tau^n} P_{p,K}^{n,k,i} + \frac{t^n-t}{\tau^n} P_{p,K}^{n-1}. \tag{5.21}$$

Note that all quantities of (5.20) and (5.21) are immediately available from the finite volume discretization of Section 5.2, more precisely on each linearization step $k \geq 1$ and each algebraic solver step $i \geq 1$ as described in Section 5.3. The simple choice in (5.20e) is motivated by [20, Remark 4.3], where $j \geq 1$ is a user-defined fixed number of additional algebraic solver iterations. A more involved choice can be made following [36]. Then no additional iterations are needed, (5.22) below holds as an inequality, and the obtained bound is typically slightly more precise.

Proceeding as for the steady linear problem in Section 3.5 while noting in particular that the chosen MPFA L-scheme verifies Assumption 3.1 in that it provides one phase pressure unknown per element, one normal flux unknown per face and per each component, and a flux balance, we can extend [20, Corollary 4.5] to:

Theorem 5.2 (Simple a posteriori error estimate distinguishing the different error components)**.** *Consider the multiphase Darcy flow according to Section 5.1, the finite volume scheme of Section 5.2, and its linearization and algebraic system solution according to Section 5.3. Let the approximate solution be understood in the sense of Section 5.4, and the error be measured in the sense of Section 5.5. Let the element matrices* $\widehat{\mathbb{A}}_{\mathrm{MFE},K}$, $\widehat{\mathbb{S}}_{\mathrm{FE},K}$, *and* $\widehat{\mathbb{M}}_{\mathrm{FE},K}$ *be respectively defined by* (3.10), (3.16), *and* (3.18). *Then*

$$\mathcal{N}^{n,k,i} \lesssim \left\{ \sum_{c \in \mathcal{C}} \left(\eta_{\mathrm{sp},c}^{n,k,i} + \eta_{\mathrm{tm},c}^{n,k,i} + \eta_{\mathrm{lin},c}^{n,k,i} + \eta_{\mathrm{alg},c}^{n,k,i} \right)^2 \right\}^{\frac{1}{2}} \tag{5.22}$$

with

$$\eta_{\mathrm{x},c}^{n,k,i} := \left\{ \delta_{\mathrm{x}} \int_{I_n} \sum_{K \in \mathcal{T}_H^n} \left(\eta_{\mathrm{x},K,c}^{n,k,i}(t) \right)^2 \mathrm{d}t \right\}^{\frac{1}{2}}, \tag{5.23}$$

where $\mathrm{x} = \mathrm{sp}, \mathrm{tm}, \mathrm{lin}, \mathrm{alg}$ *and* $\delta_{\mathrm{x}} := 2$, *except for* $\delta_{\mathrm{sp}} := 4$. *Here, for* $c \in \mathcal{C}$, *we prescribe the elementwise spatial estimators*

$$\eta_{\mathrm{sp},K,c}^{n,k,i} := \eta_{\mathrm{upw},K,c}^{n,k,i} + \left\{ \sum_{p \in \mathcal{P}_c} \left(\eta_{\mathrm{NC},K,c,p}^{n,k,i} \right)^2 \right\}^{\frac{1}{2}}, \tag{5.24a}$$

with the upwinding estimators

$$\left(\eta_{\mathrm{upw},K,c}^{n,k,i} \right)^2 := (\mathsf{U}_{\mathrm{upw},K,c}^{n,k,i})^{\mathrm{t}} \widehat{\mathbb{A}}_{\mathrm{MFE},K} (\mathsf{U}_{\mathrm{upw},K,c}^{n,k,i})$$

and the nonconformity estimators

$$\begin{aligned} \left(\eta_{\mathrm{NC},K,c,p}^{n,k,i} \right)^2 \quad := \quad & (\mathsf{U}_{K,p}^{n,k,i})^{\mathrm{t}} \widehat{\mathbb{A}}_{\mathrm{MFE},K} \mathsf{U}_{K,p}^{n,k,i} + \left(\nu_{p,K}^{n,k,i} C_{p,c,K}^{n,k,i} \right)^2 (\mathsf{S}_{K,p}^{n,k,i})^{\mathrm{t}} \widehat{\mathbb{S}}_{\mathrm{FE},K} \mathsf{S}_{K,p}^{n,k,i} \\ & + 2 \nu_{p,K}^{n,k,i} C_{p,c,K}^{n,k,i} \left[(\mathsf{U}_{K,p}^{n,k,i})^{\mathrm{t}} \mathsf{S}_{K,p}^{\mathrm{ext},n,k,i} - \sum_{\sigma \in \mathcal{E}_K} (\mathsf{U}_{K,p}^{n,k,i})_\sigma |K|^{-1} \mathbb{1}^{\mathrm{t}} \widehat{\mathbb{M}}_{\mathrm{FE},K} \mathsf{S}_{K,p}^{n,k,i} \right], \end{aligned}$$

together with the temporal estimators

$$\left(\eta_{\mathrm{tm},K,c}^{n,k,i} \right)^2 := (\mathsf{U}_{\mathrm{tm},K,c}^{n,k,i})^{\mathrm{t}} \widehat{\mathbb{A}}_{\mathrm{MFE},K} \mathsf{U}_{\mathrm{tm},K,c}^{n,k,i}, \tag{5.24b}$$

the linearization estimators

$$\left(\eta_{\mathrm{lin},K,c}^{n,k,i} \right)^2 := (\mathsf{U}_{\mathrm{lin},K,c}^{n,k,i})^{\mathrm{t}} \widehat{\mathbb{A}}_{\mathrm{MFE},K} \mathsf{U}_{\mathrm{lin},K,c}^{n,k,i} + h_K (\tau^n)^{-1} \left\| \mathcal{L}_{c,K}(\boldsymbol{\mathcal{X}}_K^{n,k,i}) - \mathcal{L}_{c,K}(\boldsymbol{\mathcal{X}}_K^{n,k-1}) - \mathcal{L}_{c,K}^{n,k,i} \right\|_{\underline{\mathbf{K}}^{-\frac{1}{2}}; L^2(K)}, \tag{5.24c}$$

and the algebraic estimators

$$\left(\eta_{\mathrm{alg},K,c}^{n,k,i} \right)^2 := (\mathsf{U}_{\mathrm{alg},K,c}^{n,k,i})^{\mathrm{t}} \widehat{\mathbb{A}}_{\mathrm{MFE},K} \mathsf{U}_{\mathrm{alg},K,c}^{n,k,i}. \tag{5.24d}$$

Proof. In order to obtain an a posteriori error estimate distinguishing the different errors components coming from the space, time, linearization, and algebraic resolutions, we proceed as in [20]. For all components $c \in \mathcal{C}$, all n, k, i, and all $K \in \mathcal{T}_H^n$, only for the purpose of this proof, we first construct some supplementary fictitious flux reconstructions:

- The *discretization flux reconstruction* $\boldsymbol{\Theta}^{n,k,i}_{\mathrm{disc},c,h}|_K \in \mathbf{RTN}_0(K)$ such that

$$\langle \boldsymbol{\Theta}^{n,k,i}_{\mathrm{disc},c,h}\cdot\boldsymbol{n}_K, 1\rangle_\sigma := \mathcal{F}_{c,K,\sigma}(\boldsymbol{\mathcal{X}}^{n,k,i}_{\mathcal{T}_H}), \qquad \forall \sigma \in \mathcal{E}^{n,\mathrm{ext}}_{K,h}, \tag{5.25a}$$

  with $\mathcal{F}_{c,K,\sigma}$ given by (5.12), while $\boldsymbol{\Theta}^{n,k,i}_{\mathrm{disc},c,h}\cdot\boldsymbol{n}_\Omega = 0$ on $\partial\Omega$.

- The *linearization error flux reconstruction* $\boldsymbol{\Theta}^{n,k,i}_{\mathrm{lin},c,h}|_K \in \mathbf{RTN}_0(K)$ such that

$$\langle \boldsymbol{\Theta}^{n,k,i}_{\mathrm{lin},c,h}\cdot\boldsymbol{n}_K, 1\rangle_\sigma = \mathcal{F}^{n,k,i}_{c,K,\sigma} - \mathcal{F}_{c,K,\sigma}(\boldsymbol{\mathcal{X}}^{n,k,i}_{\mathcal{T}_H}), \qquad \forall \sigma \in \mathcal{E}^{n,\mathrm{ext}}_{K,h}, \tag{5.25b}$$

  with $\mathcal{F}^{n,k,i}_{c,K,\sigma}$ given by (5.16), together with $\boldsymbol{\Theta}^{n,k,i}_{\mathrm{lin},c,h}\cdot\boldsymbol{n}_\Omega = 0$.

- The *algebraic error flux reconstruction* $\boldsymbol{\Theta}^{n,k,i}_{\mathrm{alg},c,h}|_K \in \mathbf{RTN}_0(K)$ such that

$$\langle \boldsymbol{\Theta}^{n,k,i}_{\mathrm{alg},c,h}\cdot\boldsymbol{n}_K, 1\rangle_{\partial K} := -\mathcal{R}^{n,k,i}_{c,K}, \qquad \forall \sigma \in \mathcal{E}^{n,\mathrm{ext}}_{K,h}, \tag{5.25c}$$

  with $\mathcal{R}^{n,k,i}_{c,K}$ defined by (5.15), while $\boldsymbol{\Theta}^{n,k,i}_{\mathrm{alg},c,h}\cdot\boldsymbol{n}_\Omega = 0$ on $\partial\Omega$.

The other degrees of freedom are then defined via a minimization solve as in Definition 3.3.

It crucially follows from (5.15), the different flux reconstructions (5.25), and the Green theorem that there holds, for all $c \in C$,

$$\left(q^n_{c,K} - \frac{\mathcal{L}_{c,K}(\boldsymbol{\mathcal{X}}^{n,k-1}_K) + \mathcal{L}^{n,k,i}_{c,K} - \mathcal{L}_{c,K}(\boldsymbol{\mathcal{X}}^{n-1}_K)}{\tau^n} - \nabla\cdot(\boldsymbol{\Theta}^{n,k,i}_{\mathrm{disc},c,h} + \boldsymbol{\Theta}^{n,k,i}_{\mathrm{lin},c,h} + \boldsymbol{\Theta}^{n,k,i}_{\mathrm{alg},c,h}), 1 \right)_K = 0 \quad \forall K \in \mathcal{T}^n_H. \tag{5.26}$$

Let $s^{n,k,i}_{h\tau} \in \mathbb{P}_1(\mathcal{T}_h)\cap H^1_0(\Omega)$ for any $t \in I_n$, be prescribed as in Definition 3.7 from the phase pressures (5.21). Then, following [20, Corollary 4.5], (5.22) holds with $\le$ instead of $\lesssim$ with (5.23) and with the local estimators given, for all components $c \in \mathcal{C}$ and all $K \in \mathcal{T}^n_H$, by ($\eta^{n,k,i}_{\mathrm{R},K,c}$ are zero here thanks to (5.26))

$$\eta^{n,k,i}_{\mathrm{sp},K,c} := \eta^{n,k,i}_{\mathrm{upw},K,c} + \left\{ \sum_{p\in\mathcal{P}_c} \left(\eta^{n,k,i}_{\mathrm{NC},K,c,p}\right)^2 \right\}^{\frac12}, \tag{5.27a}$$

$$\eta^{n,k,i}_{\mathrm{NC},K,c,p} := \nu^{n,k,i}_{p,K^\uparrow_p} C^{n,k,i}_{p,c,K^\uparrow_p} \left\| \mathbf{u}^{n,k,i}_{p,h\tau} + \underline{\mathbf{K}}\nabla s^{n,k,i}_{h\tau} \right\|_{\underline{\mathbf{K}}^{-\frac12};L^2(K)}, \tag{5.27b}$$

$$\eta^{n,k,i}_{\mathrm{upw},K,c} := \left\| \boldsymbol{\Theta}^{n,k,i}_{\mathrm{disc},c,h} - \boldsymbol{\Phi}^{n,k,i}_{c,h} \right\|_{\underline{\mathbf{K}}^{-\frac12};L^2(K)}, \tag{5.27c}$$

$$\eta^{n,k,i}_{\mathrm{tm},K,c} := \left\| \boldsymbol{\Phi}^{n,k,i}_{c,h} - \boldsymbol{\Phi}^{n,k,i}_{c,h\tau} \right\|_{\underline{\mathbf{K}}^{-\frac12};L^2(K)}, \tag{5.27d}$$

$$\eta^{n,k,i}_{\mathrm{lin},K,c} := \left\| \boldsymbol{\Theta}^{n,k,i}_{\mathrm{lin},c,h} \right\|_{\underline{\mathbf{K}}^{-\frac12};L^2(K)} + h_K(\tau^n)^{-1} \left\| \mathcal{L}_{c,K}(\boldsymbol{\mathcal{X}}^{n,k,i}_K) - \mathcal{L}_{c,K}(\boldsymbol{\mathcal{X}}^{n,k-1}_K) - \mathcal{L}^{n,k,i}_{c,K} \right\|_{\underline{\mathbf{K}}^{-\frac12};L^2(K)}, \tag{5.27e}$$

$$\eta^{n,k,i}_{\mathrm{alg},K,c} := \left\| \boldsymbol{\Theta}^{n,k,i}_{\mathrm{alg},c,h} \right\|_{\underline{\mathbf{K}}^{-\frac12};L^2(K)}. \tag{5.27f}$$

An algebraic error flux reconstruction $\boldsymbol{\Theta}^{n,k,i}_{\mathrm{alg},c,h}$ satisfying (5.25c) for an arbitrary iterative algebraic solver is developed in [36]. In practice, it is often sufficient (and much simpler) to prescribe

$$\langle \boldsymbol{\Theta}^{n,k,i}_{\mathrm{alg},c,h}\cdot\boldsymbol{n}_K, 1\rangle_\sigma = \mathcal{F}^{n,k,i+j}_{c,K,\sigma} - \mathcal{F}^{n,k,i}_{c,K,\sigma}, \qquad \forall \sigma \in \mathcal{E}^{n,\mathrm{ext}}_{K,h}, \tag{5.28}$$

for some $j \ge 1$ additional algebraic solver iterations; this satisfies the requirement (5.25c) only approximately and leads to the loss of the guaranteed upper bound in (5.22).

The bound (5.22) with the estimators given by (5.23) and (5.24) is now obtained by applying Theorem 3.12 to evaluate the nonconformity estimator given by (5.27b) and by applying Lemma 3.5 to evaluate the upwinding, temporal, linearization, and algebraic estimators of (5.27c)–(5.27f). □

6 Numerical experiments: multiphase Darcy flow

In order to validate the results of Theorem 5.2 and to test the fully adaptive Algorithm 5.1, we study here two different test cases. The first one is taken from [17], relying on the tenth SPE comparative solution project model. It is an incompressible water-oil two-phase flow problem built on a Cartesian regular geometry. This test corresponds to the layer 85 of SPE10. We choose here first the Cartesian regular mesh so as to compare our new approach with approaches already validated on this type of meshes. The second case is a simulation of a black-oil model. For this test the problem is built on a three-dimensional corner-point geometry (distorted grids), well-known and most often used in reservoir simulation due to the flexibility to permit a good representation of reservoir description, see [22] and references therein. In what follows, the proposed a posteriori error estimate framework has been implemented in a reservoir prototype simulator [38], a thermal multi-purpose simulator written in C++, which is a part of the next generation IFPEn research simulators based on the *Arcane* framework [30]. The execution platform is a public computer Intel Core i7, 8 cores, 3.7Ghz with 16GB of memory.

6.1 Two-phase flow problem

We consider a two-dimensional spatial domain discretized by a grid of 60×220 rectangular cells of size 6.096 m in the x direction and 3.048 m in the y direction. We choose the initial time step as $\tau^0 = 4.32 \times 10^4$s, which equals to 0.5 days, and the process is simulated to $t_F = 2000$ days. The reservoir is initially saturated with hydrocarbons and we consider the injection of water by a well located at the center of the grid. Four production wells are placed at the four corners of the domain. Therefore, we have a water component W and an oil component O collected in the set of components $\mathcal{C} = \{\mathrm{W}, \mathrm{O}\}$ and two phases $\mathcal{P} = \{\mathrm{w}, \mathrm{o}\}$ corresponding to water and oil. The model is actually simplified in that the components can be identified with the phases, so that $\mathcal{P}_\mathrm{W} = \{\mathrm{w}\}$ and $\mathcal{P}_\mathrm{O} = \{\mathrm{o}\}$, $C_{\mathrm{w},\mathrm{W}} = C_{\mathrm{o},\mathrm{O}} = 1$, $C_{\mathrm{o},\mathrm{W}} = C_{\mathrm{o},\mathrm{W}} = 0$, and the vector of unknowns $\boldsymbol{\mathcal{X}}$ reduces to $(P, (S_p)_{p\in\mathcal{P}})$. Note that then the accumulation term $\mathcal{L}_c$ becomes linear in the only unknown S_p, and one particular consequence is that the second term in the definition (5.24c) of $\eta^{n,k,i}_{\mathrm{lin},K,c}$ vanishes. The porosity ϕ and the permeability field $\underline{\mathbf{K}}$ (scalar coefficient times an identity matrix) are shown in Figure 8. The other parameters of Section 5.1 are given by (see [17] for more details):

- $\mu_\mathrm{o} = 10^{-3}$ Pa·s and $\mu_\mathrm{w} = 0.3 \cdot 10^{-3}$ Pa·s,
- $\zeta_\mathrm{o} = \zeta_\mathrm{w} = 1$ mole·m^{-3},
- $S_\mathrm{wi} = S_\mathrm{or} = 0.2$,
- $$k_{\mathrm{r},\mathrm{w}}(S_\mathrm{w}) = \left(\frac{S_\mathrm{w} - S_\mathrm{wi}}{1 - S_\mathrm{wi} - S_\mathrm{or}}\right)^2 \qquad \text{and} \qquad k_{\mathrm{r},\mathrm{o}}(S_\mathrm{o}) = \left(\frac{1 - S_\mathrm{o} - S_\mathrm{or}}{1 - S_\mathrm{wi} - S_\mathrm{or}}\right)^2,$$
- $P_{\mathrm{c}_p}(S_p) = 0$,
- there is no gravitational force, $z = 0$, so that the mass densities ρ_p need not be specified.

We consider a discretization by the implicit multi-point finite volume scheme of Section 5.2 with the Newton linearization detailed in Section 5.3. For the linear solver we use the Bi-Conjugated Gradient Stabilized (BiCGStab) [41] with an ILU{0} preconditioner.

Figure 9 shows, at 500 days of the simulation, the evolution of the approximate water saturation, the spatial estimator computed by the formula on Cartesian grid proposed in [48, Chapter 4], and the spatial estimator given by (5.24a). Similar behavior is observed for the two a posteriori estimators. Furthermore, we see that they both detect well the error following the saturation front despite the strong heterogeneity of the domain.

The previous result motivates an adaptive mesh refinement/coarsening (AMR) strategy based on these estimators. We now verify that the simple a posteriori estimators on polyhedral mesh of Theorem 5.2 give the expected results, while comparing it with the already validated case in [48, Chapter 4].

We first apply the AMR strategy of Algorithm 5.1 with $\zeta_\mathrm{ref} = 0.7, \zeta_\mathrm{deref} = 0.2$, and "exact" algebraic and linearization solvers. On the coarse scale, the domain is discretized by a grid of 30×110 cells and

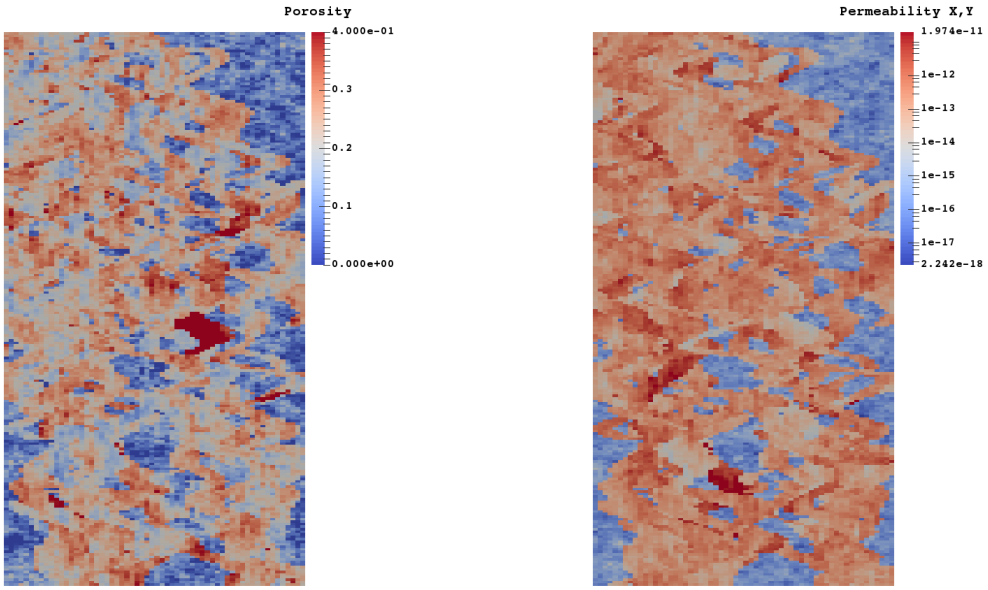

Figure 8: Porosity (*left*) and permeability (*right*), 10th SPE case

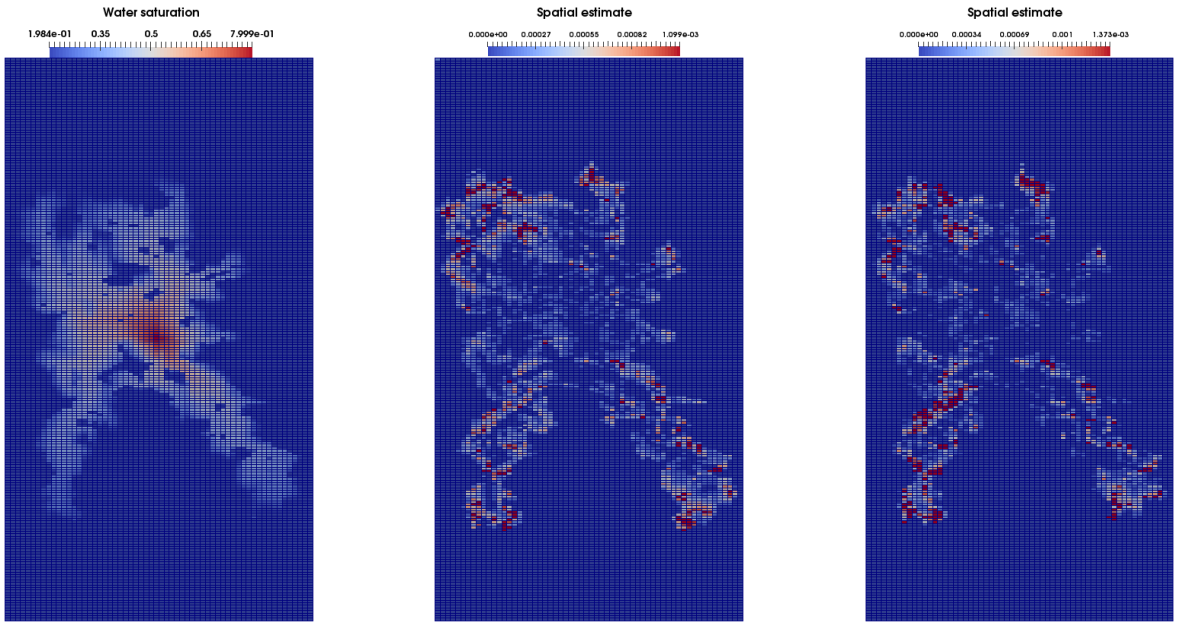

(a) Water saturation (b) Cartesian estimate of [48] (c) Polygonal simplified estimate (5.24a)

Figure 9: Two-phase flow: results at 500 days

we allow one refinement level. Figure 10 shows the evolution of the approximate water saturation at two different simulation times. We remark that the refinement follows the saturation front as times evolves. Additionally, the fact that we have a model with highly heterogeneous permeability, we are lead to perform a slow derefinement process in the zone abandoned by the front of water saturation. Figure 11 depicts the

cumulated oil rate (left) and the water-cut[1] (right) during the simulation. We compare there the results on the fine grid, the results at the coarse level, and the results with both AMR strategies. We remark that the accuracy of the results on the fine grid are almost recovered by the AMR strategy and appear much better than the coarse results.

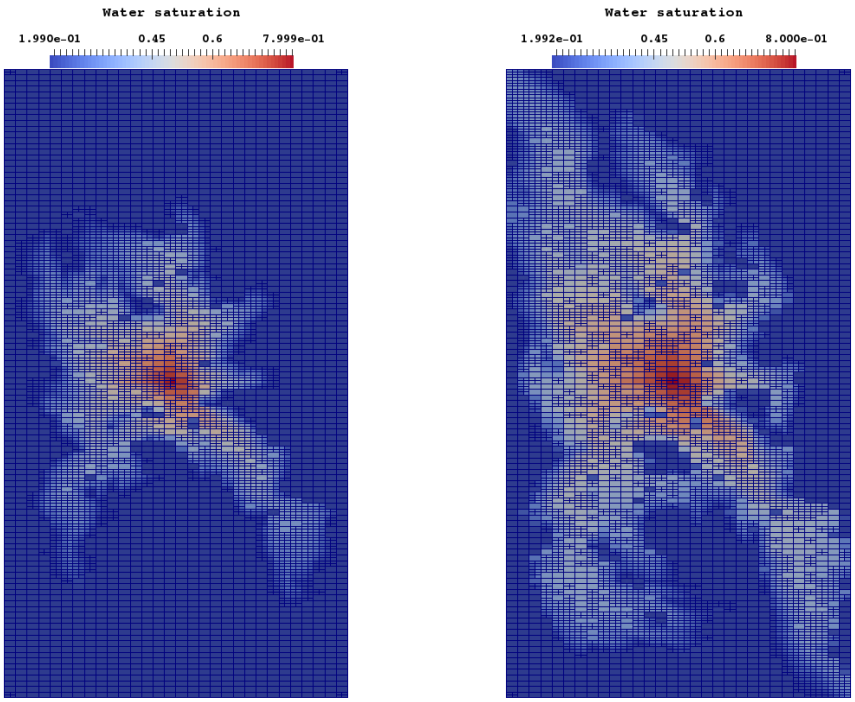

Figure 10: Two-phase flow: results at 400 days and 1100 days

The details of the efficiency of the AMR strategy based on the a posteriori error estimator can finally be appreciated in Table 1. We compare the global CPU time of the simulation for the different strategies. We detail the CPU time spent on the evaluation of the estimators and the mesh adaptation. We remark low cost of the estimators evaluation compared with the total computation CPU time, thanks to the use of the simple and fast-to-evaluate form of a posteriori error estimates on polygonal meshes of Theorem 5.2. In Table 1, when applying the mesh adaptation, the total computation CPU time is the sum of the resolution

[1]The ratio of water produced compared to the volume of total liquids produced.

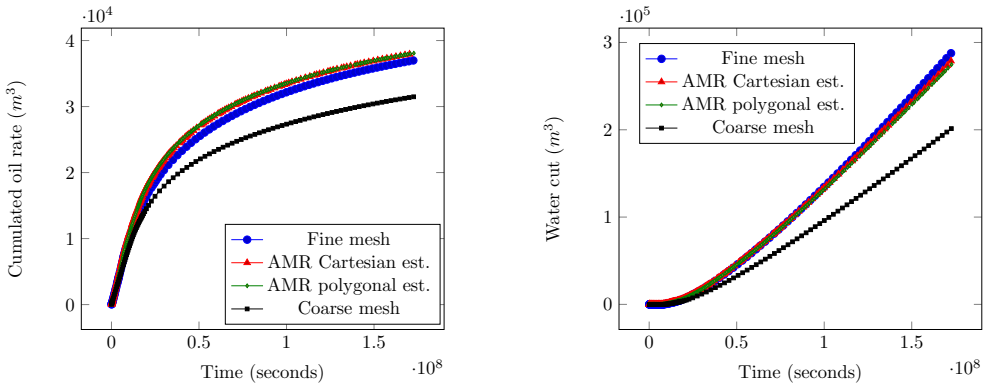

Figure 11: Fine grid vs. adaptive grid: cumulated oil rate (*left*) and water cut (*right*), two-phase flow

time, AMR time, and estimators evaluation time. We remark that applying the AMR strategy on this two-dimensional test case leads to a gain factor in the overall CPU time at around 2 wherever we use the polygonal estimate proposed in the paper or the Cartesian estimate already validated on this type of meshes. Note that, however, the simulation is slightly faster when adapting using the Cartesian estimate due to the fact that we can directly compute the **RTN** basis functions on rectangular cells.

-	Resolution	AMR	Estimators evaluation	Gain factor
Fine	603s	-	-	-
AMR Cartesian est.	229s	39s	19s	2.1
AMR polygonal est.	242s	46s	27s	1.9

Table 1: Fine grid vs. adaptive mesh refinement, two-phase flow

6.2 Three-phases, three-components problem

In this section, we present a simulation of a black-oil model. Here, we have three phases constituted by water, oil, and gas, represented by lowercase letters w, o, g as indices, respectively. The oil phase contains two types of components: nonvolatile oil and volatile oil, which we call here oil component and gas component, respectively. This is due to the fact that in this model, the hydrocarbon components are divided into light and heavy components. The light component can dissolve into the liquid oil phase or volatilize in the gas phase according to the pressure and temperature. The gas phase only contains the gas components and the water phase only contains the water component. The components are represented by uppercase letters W for the water component, O for the oil component, and G for the gas component. Therefore, we have a problem with three phases $\mathcal{P} = \{\mathrm{w}, \mathrm{o}, \mathrm{g}\}$ and three components $\mathcal{C} = \{\mathrm{W}, \mathrm{O}, \mathrm{G}\}$.

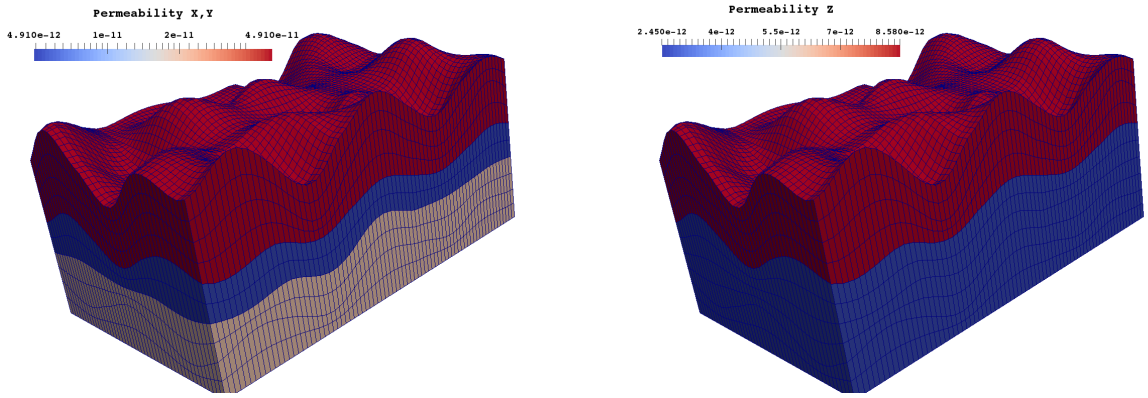

Figure 12: Permeability, black-oil model

6.2.1 Model setting

The reservoir considered in this test case is a 3-dimensional domain $\Omega := 4750\mathrm{m} \times 3000\mathrm{m} \times 114\mathrm{m}$ discretized by a corner-point geometry grid. We consider a heterogeneous anisotropic reservoir with 0.3 porosity and the permeability $\underline{\mathbf{K}}$ in a form of a diagonal matrix with the x and y components identical and forming three horizontal layers, and the z component forming two vertical permeability layers, see Figure 12. We consider a gas injection in a reservoir initially unsaturated. A vertical gas injection well perforates a corner of the reservoir in the Z direction and a production well is located in the opposite corner. On the fine scale, the domain is discretized by a grid of $76 \times 48 \times 10$ elements and on the coarse scale by a grid of $38 \times 24 \times 5$ cells, leading to one refinement level. The process is simulated to $t_F = 2000$ days with initial time step $\tau^0 = 4.32 \times 10^4$s, which equals to 0.5 days. Data, constraints, and pressure-volume properties are adapted from the first SPE comparative solution project model (SPE1) designed to simulate a three-dimensional

black-oil reservoir, given in [35, Tables 1,2, and 3]. We consider a discretization by the implicit multi-point finite volume scheme of Section 5.2 with the Newton linearization detailed in Section 5.3. For the linear solver, we again use the BiCGStab [41] with an ILU{0} preconditioner. Figure 13 shows the evolution of the gas saturation and the spatial estimator at 1000 days. Note that, for the spatial estimator, the data are normalized by max value in order to have a $[0, 1]$ range. We observe that the spatial estimator follows the saturation front though the heterogeneous anisotropic medium with time evolution.

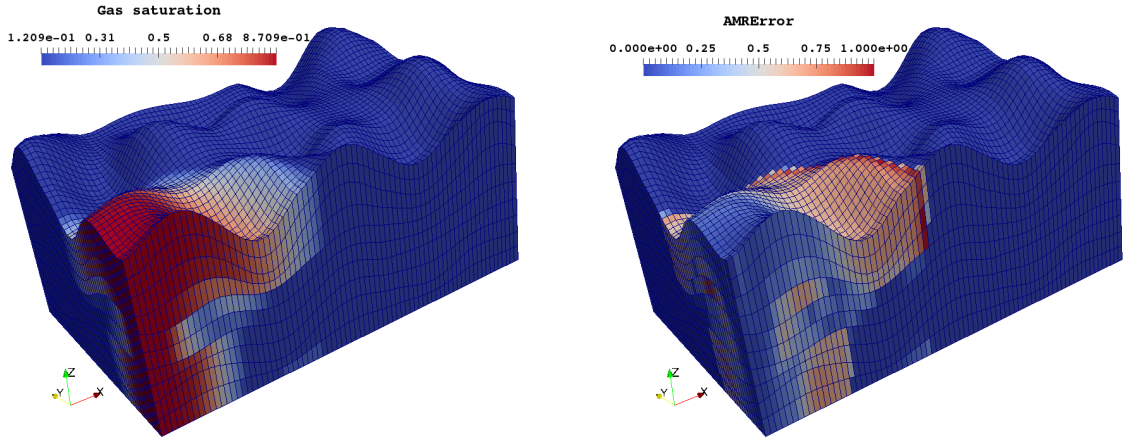

Figure 13: Results at 1000 days, gas saturation (*left*) and normalized polygonal estimate (*right*)

6.2.2 Adaptive space mesh refinement and stopping criteria for the linear solver

In the standard resolution of our reservoir prototype simulator, the chosen grid is the fine-scale one and the initial time step, as mentioned before, is chosen as $\tau^0 = 4.32 \times 10^4$s. The time step is increased systematically, by multiplying by 2, but also controlled by the convergence of the Newton linearization loop in such a way that we divide it by 2 if a divergence of the Newton algorithm occurs. We thus stick to this setting and only focus on the stopping criteria for the linear solver (and not for the Newton one) and on mesh adaptivity in space (and not in time). For the adaptive resolution, we start on the coarse-level grid allowing to one refinement level and we fix $\zeta_{\text{ref}} = 0.7, \zeta_{\text{deref}} = 0.2$. In order to compare with the standard resolution, we adopt the same mechanism of time step management and avoid the time step adaptivity and the stopping criteria for the linearization loop in Algorithm 5.1, focusing on the use of the spatial and the algebraic error estimators.

Figure 14 illustrates the evolution of the approximate gas saturation at two different time steps. We remark that the refinement follows the saturation front as times evolves. Additionally, the fact that the light component G (gas component) can dissolve into the liquid oil phase or volatilize in the gas phase, we are lead to perform some localized refinement in zones abandoned by the front of gas saturation.

We show in the left part of Figure 15, at a fixed time step 500 days and for the first Newton iteration, the evolution of the total estimator $\left(\eta_{\text{sp},c}^{n,k,i} + \eta_{\text{tm},c}^{n,k,i} + \eta_{\text{lin},c}^{n,k,i}\right)$ with, $c = \text{G}$ the gas component and $\eta_{\text{sp},c}^{n,k,i}$, $\eta_{\text{tm},c}^{n,k,i}$, and $\eta_{\text{lin},c}^{n,k,i}$ given in (5.23)–(5.24c), the algebraic estimator $\eta_{\text{alg},c}^{n,k,i}$ of (5.23), (5.24d) (with $j = 20$ in (5.28)), and the relative algebraic residual given by

$$\text{err}_{\text{alg}}^{n,k,i} := \frac{\left\| A^{n,k-1} X^{n,k,i} - b^{n,k-1} \right\|}{\left\| b^{n,k-1} \right\|}$$

with $A^{n,k-1} X^{n,k} = b^{n,k-1}$ being the linear system resulting from the k-th iteration of the Newton method at time step t^n, see Section 5.3. For the standard resolution, we stop the algebraic iteration using a fixed

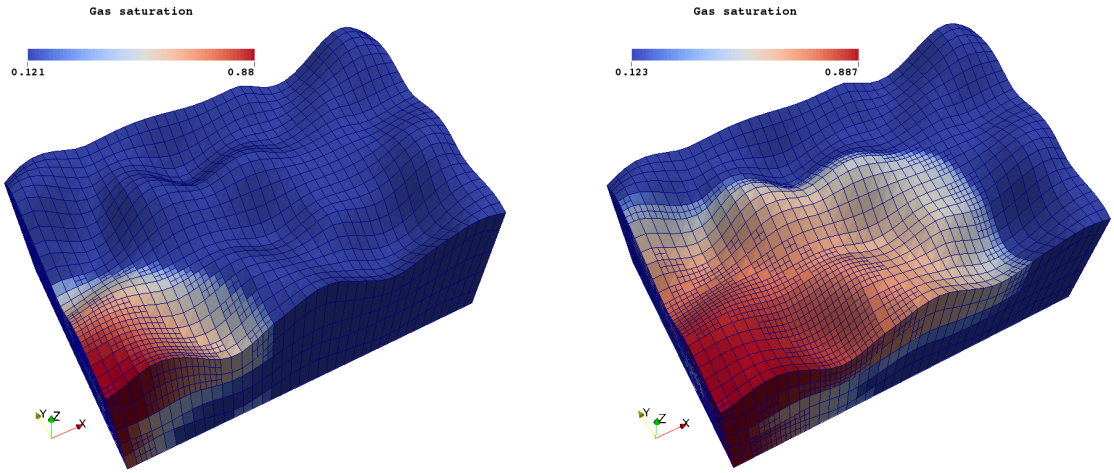

Figure 14: Gas saturation: results at 500 days (*left*) and 1500 days (*right*), black-oil model

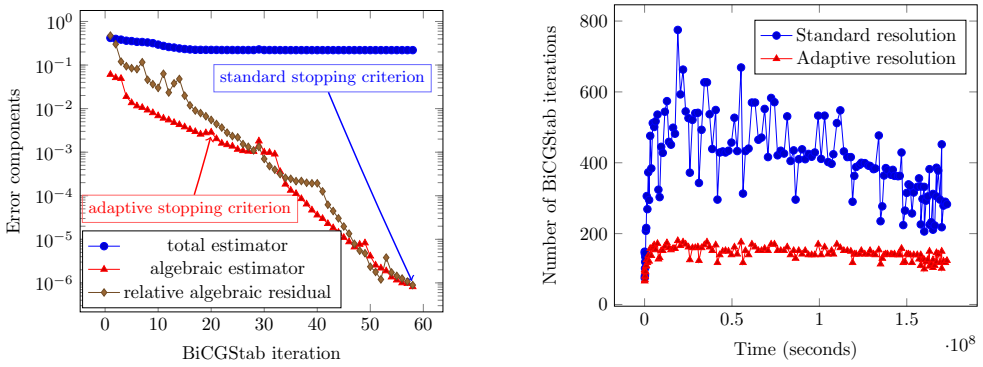

Figure 15: Standard resolution vs. adaptive resolution: total estimator and its algebraic component (*left*) and number of BiCGStab iterations per time step (*right*), black-oil model

threshold $\mathrm{err}_{\mathrm{alg}}^{n,k,i} \leq 10^{-6}$, following our usual practice. In the adaptive resolution based on Algorithm 5.1, we fix $\gamma_{\mathrm{alg}} = 10^{-2}$.

We remark, in the left part of Figure 15, that the algebraic estimator steadily decreases, while the total estimator almost stagnates after about a half of total number of iterations necessary to converge using the standard stopping criterion. In the right part of Figure 15, we depict the cumulated number of BiCGStab iterations at each time step (the sum of the necessary number of BiCGStab iterations at each Newton iteration of the time step). We observe a significant gain.

We compare in Figure 16 the number of cells and the cumulated rate of oil production resulting from both the standard and the adaptive resolution. We can observe in the left part of Figure 16 that the adaptive algorithm does not have any significant influence on the accuracy of production. The right part of Figure 16 shows an important reduction in the number of cells via the adaptive resolution compared with the standard one.

The necessary linear solver steps and the different CPU times of the adaptive and standard resolutions are collected in Table 2. It shows that the total number of linear solver steps is reduced by 70%, which is an important gain. An important gain is also observed in CPU time. We in particular remark that the time spent for the adaptation (AMR and estimators evaluation) only represents a small part of the actual resolution time. Globally, a reduction factor of 3.8 of the overall CPU time is obtained by comparing the adaptive resolution with the standard one. Important increase of this reduction factor is still to be expected when also the Newton solver stopping criteria and time step adaptation are used.

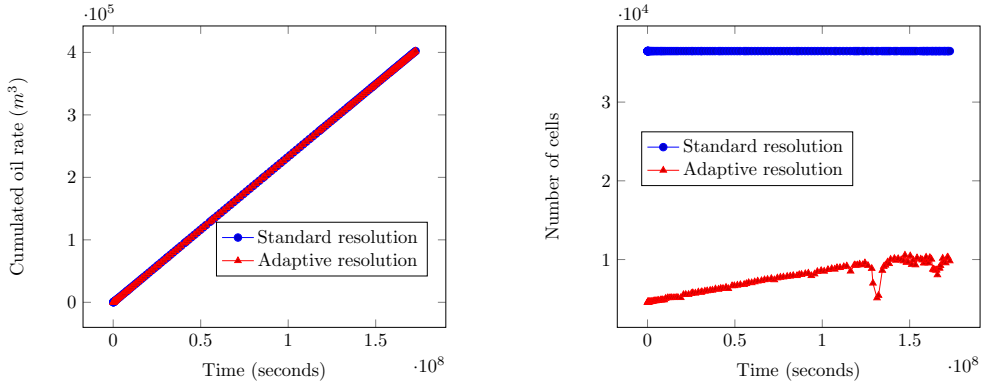

Figure 16: Standard resolution vs. adaptive resolution: cumulated oil rate (*left*) and number of cells (*right*), black-oil model

	Linear solver steps	**Resolution time**	**AMR time**	**Estimators evaluation**	**Gain factor**
Standard resolution	66386	1023s	-	-	-
Adaptive resolution	20184	201s	42s	26s	3.8

Table 2: Comparison between standard and adaptive resolutions, black-oil model

7 Conclusions

This paper presents a posteriori error estimates that can be readily implemented into (reservoir engineering) production codes on general polytopal meshes with a minimal overhead. These estimates allow for a very fast evaluation and, according to Theorem 3.12, give a guaranteed control over the error committed in the approximation of the exact Darcy velocity (flux) for the steady linear single-phase Darcy flow. Theorem 5.2 then gives a similar result for unsteady multiphase Darcy flows. Here, additionally, all the different error components (time and space discretizations, linearization, algebraic) are identified, leading to a proposition of a fully adaptive algorithm with all adaptive stopping criteria for linear and nonlinear solvers, adaptive time step management, and adaptive mesh refinement. Numerical experiments on real-life problems confirm important speed-ups that can be achieved with our methodology, in addition to the certification of the computed output.

References

[1] I. Aavatsmark, G. T. Eigestad, R. A. Klausen, M. F. Wheeler, and I. Yotov, *Convergence of a symmetric MPFA method on quadrilateral grids*, Comput. Geosci., 11 (2007), pp. 333–345.

[2] Y. Achdou, C. Bernardi, and F. Coquel, *A priori and a posteriori analysis of finite volume discretizations of Darcy's equations*, Numer. Math., 96 (2003), pp. 17–42.

[3] M. Ainsworth, *Robust a posteriori error estimation for nonconforming finite element approximation*, SIAM J. Numer. Anal., 42 (2005), pp. 2320–2341.

[4] P. F. Antonietti, L. Beirão da Veiga, C. Lovadina, and M. Verani, *Hierarchical a posteriori error estimators for the mimetic discretization of elliptic problems*, SIAM J. Numer. Anal., 51 (2013), pp. 654–675.

[5] Y. Bazilevs, L. Beirão da Veiga, J. A. Cottrell, T. J. R. Hughes, and G. Sangalli, *Isogeometric analysis: approximation, stability and error estimates for h-refined meshes*, Math. Models Methods Appl. Sci., 16 (2006), pp. 1031–1090.

[6] L. Beirão da Veiga, *A residual based error estimator for the mimetic finite difference method*, Numer. Math., 108 (2008), pp. 387–406.

[7] L. Beirão da Veiga, F. Brezzi, A. Cangiani, G. Manzini, L. D. Marini, and A. Russo, *Basic principles of virtual element methods*, Math. Models Methods Appl. Sci., 23 (2013), pp. 199–214.

[8] L. Beirão da Veiga and G. Manzini, *An a posteriori error estimator for the mimetic finite difference approximation of elliptic problems*, Internat. J. Numer. Methods Engrg., 76 (2008), pp. 1696–1723.

[9] L. Beirão da Veiga and G. Manzini, *Residual a posteriori error estimation for the virtual element method for elliptic problems*, ESAIM Math. Model. Numer. Anal., 49 (2015), pp. 577–599.

[10] J. Bonelle and A. Ern, *Analysis of compatible discrete operator schemes for elliptic problems on polyhedral meshes*, ESAIM Math. Model. Numer. Anal., 48 (2014), pp. 553–581.

[11] F. Brezzi and M. Fortin, *Mixed and hybrid finite element methods*, vol. 15 of Springer Series in Computational Mathematics, Springer-Verlag, New York, 1991.

[12] F. Brezzi, K. Lipnikov, and M. Shashkov, *Convergence of the mimetic finite difference method for diffusion problems on polyhedral meshes*, SIAM J. Numer. Anal., 43 (2005), pp. 1872–1896.

[13] A. Buffa and C. Giannelli, *Adaptive isogeometric methods with hierarchical splines: error estimator and convergence*, Math. Models Methods Appl. Sci., 26 (2016), pp. 1–25.

[14] E. Burman and A. Ern, *Continuous interior penalty hp-finite element methods for advection and advection-diffusion equations*, Math. Comp., 76 (2007), pp. 1119–1140.

[15] C. Cancès, I. S. Pop, and M. Vohralík, *An a posteriori error estimate for vertex-centered finite volume discretizations of immiscible incompressible two-phase flow*, Math. Comp., 83 (2014), pp. 153–188.

[16] A. Cangiani, E. H. Georgoulis, and P. Houston, *hp-version discontinuous Galerkin methods on polygonal and polyhedral meshes*, Math. Models Methods Appl. Sci., 24 (2014), pp. 2009–2041.

[17] M. Christie and M. Blunt, *Tenth SPE comparative solution project: A comparison of upscaling techniques*, in SPE Reservoir Simulation Symposium, Society of Petroleum Engineers, 2001.

[18] K. H. Coats et al., *Implicit compositional simulation of single-porosity and dual-porosity reservoirs*, in SPE Symposium on Reservoir Simulation, Society of Petroleum Engineers, 1989.

[19] B. Cockburn, D. A. Di Pietro, and A. Ern, *Bridging the hybrid high-order and hybridizable discontinuous Galerkin methods*, ESAIM Math. Model. Numer. Anal., 50 (2016), pp. 635–650.

[20] D. A. Di Pietro, E. Flauraud, M. Vohralík, and S. Yousef, *A posteriori error estimates, stopping criteria, and adaptivity for multiphase compositional Darcy flows in porous media*, J. Comput. Phys., 276 (2014), pp. 163–187.

[21] D. A. Di Pietro, M. Vohralík, and S. Yousef, *An a posteriori-based, fully adaptive algorithm with adaptive stopping criteria and mesh refinement for thermal multiphase compositional flows in porous media*, Comput. Math. Appl., 68 (2014), pp. 2331–2347.

[22] Y. Ding and P. Lemonnier, *Use of corner point geometry in reservoir simulation*, Society of Petroleum Engineers, (1995).

[23] J. Droniou, R. Eymard, T. Gallouët, and R. Herbin, *A unified approach to mimetic finite difference, hybrid finite volume and mixed finite volume methods*, Math. Models Methods Appl. Sci., 20 (2010), pp. 265–295.

[24] R. Durán and C. Padra, *An error estimator for nonconforming approximations of a nonlinear problem*, in Finite element methods (Jyväskylä, 1993), vol. 164 of Lecture Notes in Pure and Appl. Math., Dekker, New York, 1994, pp. 201–205.

[25] A. Ern and M. Vohralík, *Flux reconstruction and a posteriori error estimation for discontinuous Galerkin methods on general nonmatching grids*, C. R. Math. Acad. Sci. Paris, 347 (2009), pp. 441–444.

[26] ——, *Adaptive inexact Newton methods with a posteriori stopping criteria for nonlinear diffusion PDEs*, SIAM J. Sci. Comput., 35 (2013), pp. A1761–A1791.

[27] ——, *Polynomial-degree-robust a posteriori estimates in a unified setting for conforming, nonconforming, discontinuous Galerkin, and mixed discretizations*, SIAM J. Numer. Anal., 53 (2015), pp. 1058–1081.

[28] R. Eymard, T. Gallouët, and R. Herbin, *Finite volume approximation of elliptic problems and convergence of an approximate gradient*, Appl. Numer. Math., 37 (2001), pp. 31–53.

[29] R. Eymard, C. Guichard, R. Herbin, and R. Masson, *Vertex-centred discretization of multiphase compositional darcy flows on general meshes*, Computational Geosciences, 16 (2012), pp. 987–1005.

[30] G. Grospellier and B. Lelandais, *The Arcane development framework*, in Proceedings of the 8th workshop on Parallel/High-Performance Object-Oriented Scientific Computing, POOSC '09, New York, NY, USA, 2009, ACM, pp. 4:1–4:11.

[31] O. A. Karakashian and F. Pascal, *A posteriori error estimates for a discontinuous Galerkin approximation of second-order elliptic problems*, SIAM J. Numer. Anal., 41 (2003), pp. 2374–2399.

[32] Y. Kuznetsov and S. Repin, *New mixed finite element method on polygonal and polyhedral meshes*, Russian J. Numer. Anal. Math. Modelling, 18 (2003), pp. 261–278.

[33] Y. A. Kuznetsov, *Mixed finite element methods on polyhedral meshes for diffusion equations*, in Partial differential equations, vol. 16 of Comput. Methods Appl. Sci., Springer, Dordrecht, 2008, pp. 27–41.

[34] W. F. Mitchell, *A collection of 2D elliptic problems for testing adaptive grid refinement algorithms*, Applied Mathematics and Computation, 220 (2013), pp. 350–364.

[35] A. S. Odeh, *Comparison of solutions to a three-dimensional black-oil reservoir simulation problem (includes associated paper 9741)*, Journal of Petroleum Technology, 33 (1981), pp. 13–25.

[36] J. Papež, U. Rüde, M. Vohralík, and B. Wohlmuth, *Sharp algebraic and total a posteriori error bounds via a multilevel approach*. In preparation, 2017.

[37] W. Prager and J. L. Synge, *Approximations in elasticity based on the concept of function space*, Quart. Appl. Math., 5 (1947), pp. 241–269.

[38] O. Ricois, *Vision générale du simulateur ARCEOR*, tech. rep., IFPEN, 2011.

[39] J. E. Roberts and J.-M. Thomas, *Mixed and hybrid methods*, in Handbook of Numerical Analysis, Vol. II, North-Holland, Amsterdam, 1991, pp. 523–639.

[40] A. Sboui, J. Jaffré, and J. Roberts, *A composite mixed finite element for hexahedral grids*, SIAM J. Sci. Comput., 31 (2009), pp. 2623–2645.

[41] H. A. van der Vorst, *Bi-CGSTAB: a fast and smoothly converging variant of Bi-CG for the solution of nonsymmetric linear systems*, SIAM J. Sci. Statist. Comput., 13 (1992), pp. 631–644.

[42] M. Vohralík, *A posteriori error estimates for lowest-order mixed finite element discretizations of convection-diffusion-reaction equations*, SIAM J. Numer. Anal., 45 (2007), pp. 1570–1599.

[43] ——, *Residual flux-based a posteriori error estimates for finite volume and related locally conservative methods*, Numer. Math., 111 (2008), pp. 121–158.

[44] ——, *Unified primal formulation-based a priori and a posteriori error analysis of mixed finite element methods*, Math. Comp., 79 (2010), pp. 2001–2032.

[45] M. Vohralík and M. F. Wheeler, *A posteriori error estimates, stopping criteria, and adaptivity for two-phase flows*, Comput. Geosci., 17 (2013), pp. 789–812.

[46] M. Vohralík and B. I. Wohlmuth, *Mixed finite element methods: implementation with one unknown per element, local flux expressions, positivity, polygonal meshes, and relations to other methods*, Math. Models Methods Appl. Sci., 23 (2013), pp. 803–838.

[47] M. Wheeler, G. Xue, and I. Yotov, *A multipoint flux mixed finite element method on distorted quadrilaterals and hexahedra*, Numer. Math., 121 (2012), pp. 165–204.

[48] S. Yousef, *A posteriori error estimates and adaptivity based on stopping criteria and adaptive mesh refinement for multiphase and thermal flows. Application to steam-assisted gravity drainage*, Ph.D. thesis, Université Pierre et Marie Curie - Paris VI, 2013.